

Stratigraphy, palaeontology and geochemistry of the late Neoproterozoic Aar Member, southwest Namibia: Reflecting environmental controls on Ediacara fossil preservation during the terminal Proterozoic in African Gondwana[☆]



Michael Hall^a, Alan J. Kaufman^b, Patricia Vickers-Rich^{a,*}, Andrey Ivantsov^{a,c}, Peter Trusler^a, Ulf Linnemann^d, Mandy Hofmann^d, David Elliott^a, Huan Cui^b, Mikhail Fedonkin^{a,c}, Karl-Heinz Hoffmann^e, Siobhan A. Wilson^a, Gabi Schneider^e, Jeff Smith^a

^a School of Geosciences, Monash University, Clayton, Vic. 3800, Australia

^b Department of Geology and Earth System Science Interdisciplinary Center, University of Maryland, College Park, MD 20742-4211, USA

^c Paleontological Institute, Russian Academy of Sciences, Profsoyuznaya ul. 123, Moscow 117997, Russia

^d Senckenberg Naturhistorische Sammlungen Dresden, Geochronology Section (GeoPlasma Lab), Koenigsbruecker Landstrasse 159, D-01109 Dresden, Germany

^e Namibian Geological Survey, Ministry of Mines and Energy, Windhoek, Namibia

ARTICLE INFO

Article history:

Received 19 December 2012

Received in revised form 3 September 2013

Accepted 6 September 2013

Available online xxx

Keywords:

Nama Group

Ediacaran

Kliphoek Sandstone

Pteridinium

Rangea

Isotope geochemistry

Neoproterozoic

ABSTRACT

Common, Ediacaran fossils are well preserved in a Late Neoproterozoic (ca. 545 Ma) shallow marine sequence, described here as the Aar Member of the Dabis Formation (Kuibis Subgroup, Nama Group), near Aus in southwest Namibia. This 31–38 m thick, shale-dominant unit records the transition from fluvial-shallow marine Kliphoek Sandstone to open marine limestone of the Mooifontein Member of the Zaris Formation, deposited on a subsiding continental margin during a major, regional transgression. Thin sandstone beds contain fossils at a number of levels throughout the Aar Member. Concentrations of *Pteridinium* were mostly transported in flood-derived sheets, while some *Ernietta* assemblages are preserved close to *in situ*. *Rangea* has also been transported, and is mostly confined to thin sandstone lenses incised into mudstone. Limestone beds, common throughout, include at least two marker horizons that can be followed regionally and show local evidence of storm reworking. Systematic sampling and analyses of limestone reveals enrichment in both ^{13}C and ^{18}O higher in the section, with negative $\delta^{13}\text{C}$ near the base rising to moderate positive values near the top. The negative-to-positive transition in $\delta^{13}\text{C}$ values is more pronounced in the east, with all of the lower Aar Member samples consistently depleted in ^{13}C . While this may reflect greater degrees of alteration by meteoric or dewatering fluids, the same carbonates are notably enriched in ^{18}O relative to those at the same stratigraphic position to the west. The overall rise in ^{13}C is attributed to greater proportional burial of organic matter and release of oxygen to surface environments, while the spatial variability is likely the result of a strong surface-to-deep carbon isotopic gradient in seawater. A number of the fossils, especially *Rangea*, are encrusted with jarosite, an iron-bearing sulphate mineral and common weathering product of pyrite. This observation suggests that preservation of the fossils may have resulted from the rapid encrustation of pyrite on the surface of the organisms as they decomposed and were consumed by sulphate-reducing bacteria within the sandy, near shore sediments. Insofar as pyrite formation requires iron, which is soluble and reactive in anoxic solutions, it is likely that the deeper subtidal environments lacked oxygen. *In situ* pyritized forms like *Ernietta* may have developed the capacity to survive under episodically anoxic or sub-oxic environmental conditions, while *Pteridinium* and *Rangea* lived within an oxygenated estuarine or fluvial setting and were transported during storms to anoxic, ferruginous environments where they were exquisitely preserved.

© 2013 The Authors. Published by Elsevier B.V. All rights reserved.

[☆] This is an open-access article distributed under the terms of the Creative Commons Attribution-NonCommercial-No Derivative Works License, which permits non-commercial use, distribution, and reproduction in any medium, provided the original author and source are credited.

* Corresponding author. Tel.: +61 399054889.

E-mail address: Pat.Rich@monash.edu (P. Vickers-Rich).

1. Introduction

The recent discovery of over one hundred exquisitely preserved specimens of the late Ediacaran Period fossil *Rangea* (Vickers-Rich et al., 2013) on Farm Aar in southwest Namibia prompted new sedimentological and geochemical investigations of uppermost Kuibis Subgroup strata (ca. 550–555 Ma; Grotzinger et al., 1995; 545–548 Ma; Narbonne et al., 2012). The investigated stratigraphic interval preserves carbon and sulphur isotope evidence of significant environmental change, which is considered here in context of the evolution, diversification, and taphonomy of Earth's earliest metazoans. In particular, morphologic details of the newly discovered *Rangea* fossils are preserved in jarosite (an iron-bearing sulfate mineral) coatings, which are likely the oxidative weathering products of early diagenetic pyrite (e.g., Gehling, 1999). Astrobiological interest in jarosite stems from its presence on the surface of Mars, which potentially indicates wet, acid, and sulfate-rich conditions early in planetary history (Squyres et al., 2004). In association with these Ediacara fossils, jarosite may be related to environmental contrasts between deep and shallow marine settings and their unusual mode of preservation.

The oldest examples of the late Neoproterozoic Ediacara biota in the Kuibis Subgroup occur in strata that preserve a globally recognized positive carbonate carbon isotope anomaly (Kaufman et al., 1991; Saylor et al., 1998). Insofar as these events reflect the greater proportional sequestration of organic matter in sediments and release of oxidants (Hayes, 1983), the first appearance of the Ediacara biota in Namibia may be directly associated with the rise of oxygen in shallow marine environments. In this study we analyzed the carbon, oxygen, and sulphur isotope compositions of carbonate and siliciclastic samples from three closely spaced sections through a transitional interval, which is here newly defined as the Aar Member of the Kuibis Subgroup. In order to further understand environmental change coincident with the origination and evolution of the Ediacara biota, time-series trends in carbon isotope abundances were compared against fossil distributions in the Aar Member.

2. Regional geology

Deposition of Ediacaran Period sediments on the Kalahari Craton, including the Witvlei and Nama groups and their lateral equivalents, is described as occurring in a foreland basin that developed during convergence of the Damara and Gariep fold belts (Germs, 1983, 1995; Gresse and Germs, 1993). Saylor (1993), Saylor and Grotzinger (1997), and Saylor et al. (1995, 1998, 2005) provided a detailed sequence stratigraphic framework that placed glacial horizons (Hoffmann, 1989; Kaufman et al., 1991) and a diverse assemblage of terminal Neoproterozoic fossils, including traces of the Ediacara biota and the earliest biomimetic organisms (Crimes and Germs, 1982; Germs, 1983; Grant, 1990; Grotzinger et al., 1995, 2000) in the context of radiometric age constraints (Grotzinger et al., 1995) and profound carbon and strontium isotope variations (Kaufman et al., 1991, 1993, 1997; Derry et al., 1992; Jacobsen and Kaufman, 1999).

The fossiliferous Nama Group has been further subdivided into the Kuibis and Schwarzrand subgroups (Fig. 1). Typical late Ediacaran Period fossils, including forms such as *Ernietta*, *Pteridinium*, *Swartpuntia*, and *Rangea* (Pflug, 1966, 1970a, 1970b, 1972; Germs, 1972, 1983; Grazhdankin and Seilacher, 2005; Grotzinger et al., 1995; Narbonne et al., 1997; Pflug, 1966, 1970a, 1970b, 1972), vendotaenids (Germs et al., 1986), *Cloudina* (Germs, 1983; Grant, 1990) plus other calcified fossils (Grotzinger et al., 1995, 2000) and carbonized remains (Leonov et al., 2010), have been recovered from sediments both north and south of the palaeostructural high

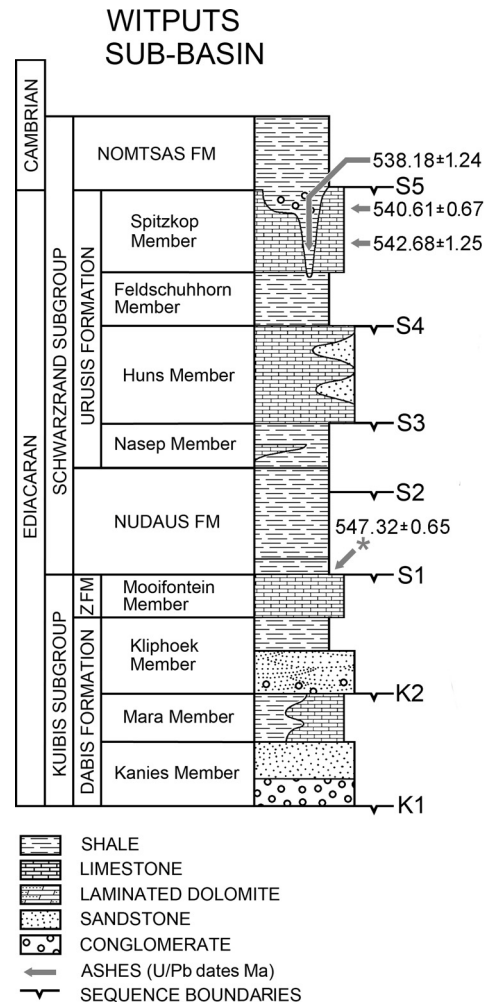


Fig. 1. Regional Stratigraphy of the Nama Group, southern Namibia, showing the positions of the newly named Aar Member and renamed Kliphoek Sandstone, subdivisions of the original Kliphoek Member.

Osis Ridge in the Zaris and Witputs sub-basins, respectively. The stratigraphically youngest Ediacara-type fossils, including *Swartpuntia*, lie 60 m below the Ediacaran–Cambrian boundary in the more southerly portion of the Witputs sub-basin (Narbonne et al., 1997), while the oldest occur in the Mara Member of the Kuibis Subgroup (Saylor et al., 1995).

The Kuibis Subgroup, the focus of this study, is thickest near the Damara and Gariep fold belts and thins until the subgroup completely disappears over the Osis Ridge (Germs, 1983, 1995; Gresse and Germs, 1993). The subgroup has been further subdivided into the sandstone-dominated Dabis and carbonate-dominated Zaris formations, which comprise three unconformity-bounded sequences. Relevant to this study are the K1 and K2 sequences. In the region around Farm Aar, K1 comprises the Kanies Member of the Dabis Formation, which unconformably overlies crystalline basement and includes a basal unit of coarse, tabular-bedded sandstones with small wave-generated ripples and desiccation cracks interpreted as tidal-flat deposits. The upper part of K1 above the Kanies Member is the carbonate-dominated Mara Member, which contains the oldest reported remains of *Cloudina* in the Namibian stratigraphy. Carbonates in the K1 sequence are uniformly depleted in $\delta^{13}\text{C}$ with $\delta^{13}\text{C}$ values as low as $-6\text{\textperthousand}$ (Kaufman et al., 1991; Saylor et al., 1998; Ries et al., 2009). In contrast, sequence K2 is typified by upward-increasing $\delta^{13}\text{C}$ values that define the rising limb of a positive excursion. In the Witputs sub-basin K2 is represented by

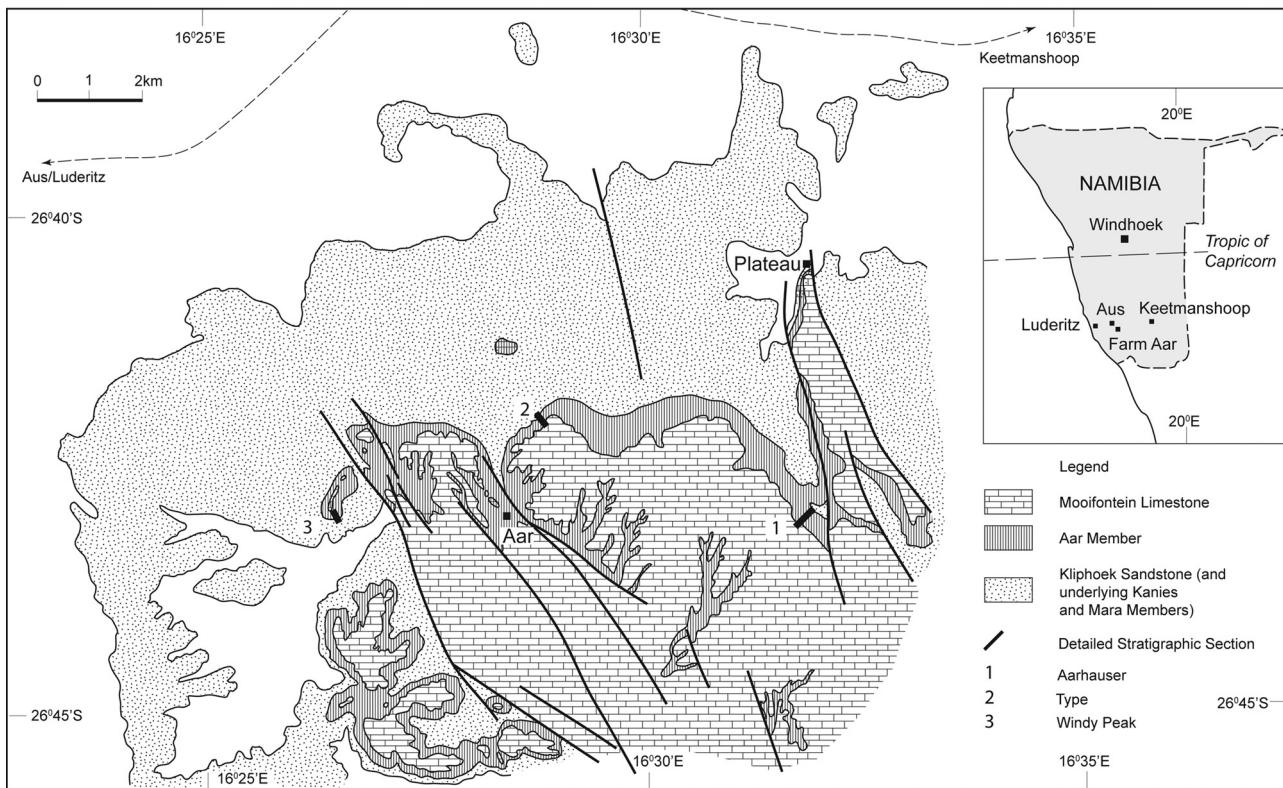


Fig. 2. Location and Geological Map, showing positions of the detailed stratigraphic sections measured on Farm Aar.

siliciclastics of the Kliphoek Member and overlying Mooifontein Member of the Zaris Formation. The sandstones are thick, tabular units, medium-grained and cross-bedded, containing abundant, basement-derived lithic fragments, and were interpreted by Saylor et al., 1995 as upper-shoreface, delta- or tide-influenced deposits that prograded across the underlying carbonate platform during sea level lowstand and were trapped during regional transgression of the craton. The upper part of K2 forms an extensive carbonate platform that maintains a relatively constant thickness (30–40 m) over the Witputs sub-basin, pinching out only in the immediate vicinity of the Osis Ridge. South of the Osis Ridge sequence K2 carbonates constitute the Mooifontein Member, a thin-bedded limestone with graded beds, ripple lamination, and intraclast breccias interpreted as storm reworking. Saylor et al. (1998) commented that little change in the thickness of these facies suggests deposition across a broad region of low relief during flooding of the craton. South of the Osis Ridge K2 is truncated by an unconformity with deep canyons cutting into the Mooifontein Member and filled with conglomerate and overlain by basal siliciclastics of the Schwarzrand Subgroup.

3. Aar Member

On Farm Aar, basal sediments of the Nama Group rest unconformably on crystalline basement immediately south of the Luderitz-Keetmanshoop Highway (B4) east of Aus (Fig. 2). The sediments form a prominent scarp capped by a gently sloping plateau underlain by sandstone of the lower part of the Kliphoek Member (and older units). Further south another scarp, capped by Mooifontein Member limestone, underlies a higher-level plateau surface. The scarp beneath the limestone results from the preferential erosion of less resistant sediments that form a distinct, regionally traceable unit, here defined as the Aar Member of the Dabis Formation. These sediments dip gently southwards and are cut by a number of north-to-northwest trending normal faults with

displacements of up to 70 m. Small-scale folds with limbs dipping up to 60° occur close to some faults indicate that the area has suffered mild compressional deformation, probably during the Damara-Gariep Orogeny.

In order to formally establish the Aar Member, six complete stratigraphic sections and a number of partial sections were measured in detail across an outcrop width of 8.5 km approximately 20 km ESE of Aus. Mapping of areas along this transect, especially where fossils are abundant, was carried out at scales varying from 1:500 to 1:5000. The newly described Aar Member has previously been referred to as the Buchholzbrunn Member by Germs and Gresse (1991) and the upper Kliphoek Member of the Dabis Formation (Saylor et al., 1998) lying between the top of the lower part of the Kliphoek Member and the base of the Mooifontein Member. The lower part of the Kliphoek Member is also revised here to include only the sandstone and very minor shale that underlies the newly defined Aar Member, and the more meaningful name Kliphoek Sandstone is now used to denote this unit. Because of their areal extent, thickness, ease of recognition, and fossil assemblages, the Aar and Kliphoek sandstone members should be redefined as formations in the future. It should also be noted that in the Farm Aar region the underlying Karies and Mara members of the Dabis Formation are intercalated and will also require future redefinition.

The newly named Aar Member is 31–38 m thick and dominated by interbedded shale and limestone. It is most commonly exposed on steep slopes capped by the Mooifontein Member but is usually covered by varying amounts of limestone scree, so that the dominant shale component is only poorly exposed. Limestone beds, particularly the thicker, upper units, are the most conspicuous features of all outcrops and form prominent benches that can be traced for many kilometres (Fig. 3). The underlying Kliphoek Sandstone is comprised dominantly of well-bedded, medium to fine-grained sandstone with common tabular cross stratified beds up to 20 cm thick, of probable fluvial deposition, and, at the top, asymmetric



Fig. 3. Typical outcrop of Aar Member, showing benches formed by carbonate beds; hilltop is capped by limestone of the Mooifontein Member; north of Windy Peak.

ripple marks with some interference ripples, indicative of reworking in a shallow marine setting. The dominant sediment transport direction was towards the south and southwest. *Pteridinium* and *Ernietta*, along with rare *Rangea*, occur locally in the uppermost 1 m of the sandstone.

4. Type section description

The type section of our Aar Member is located approximately 2.0 km north-northeast of Farm Aar homestead (Fig. 4) referred to by Leonov et al. (2010) as Road Quarry 2.3. Supplementary reference sections (Fig. 5) are located at Aarhauser (5.5 km to the east) and at Windy Peak (3.0 km to the west). Other sections have been measured on the scarp northeast of the homestead, in the Ernietta Hill area east of Windy Peak, and in valleys to the southwest and southeast. In general, the stratigraphy described below is maintained over an extensive region and varies only in the number and thickness of carbonate and sandstone beds and slight changes in overall thickness. Exact locations for these sections are on file in records of the Namibian Geological Survey, Windhoek.

The basal 2–4 m of the Aar Member, lying beneath the lowermost limestone bed, are dominated by green-grey to brown and partly maroon shale with thin, lenticular beds of fine to very fine-grained sandstone with scattered muscovite flakes (Fig. 6a). Sandstone beds are up to 22 cm thick and as thin as 0.5 cm, but mostly less than 5 cm thick and vary in outcrop extent from 1 m to 15 m. There is no clear relationship between thickness and lateral extent of these beds, which typically have wedge-shaped terminations. Most have sharp bases that may be slightly undulating and cut down as much as 3 cm into the underlying shale. They also have sharp tops that can also be slightly undulating, but a few of the beds fine upwards from very fine-grained sandstone into shale. The sandstones are typically internally laminated and locally exhibit rare, small-scale ripple cross laminations. Fossils preserved in the basal part of the Aar Member include concentrations of *Rangea*, while the shales above the *Rangea*-rich lenses host a variety of carbonaceous materials, some algae (Leonov et al., 2010) and other yet undescribed organic remains.

The overlying 4–5 m of the section are dominated by interbedded shale and thin limestone beds with some thin, fine to very fine-grained sandstone (strictly quartzite) beds, some with ripple marks on their upper surface. The limestone beds are typically olive-brown, up to 40 cm thick but mostly less than 20 cm, and have sharp bases and tops. The thicker beds commonly pinch and swell slightly along strike, while some of the thinnest carbonate beds pinch out.

Above this is 1.5–2 m dominated by up to eight, mostly fine-grained, micaceous sandstone beds up to 35 cm thick (here designated the Aarhauser Sandstone sub-member). This sandstone contains locally abundant *Pteridinium* fossil concentrations (Vickers-Rich et al., 2013) and rare occurrences of *Rangea* and has been traced laterally for up to 6 km along strike east of the type section, but is not continuously exposed. Both taxa also occur rarely in isolated ironstone concretions within this member northwest of Aarhauser. Most of the sandstone beds are strongly laminated, but examples of low angle cross beds were also observed, mostly in blocks, although one *in situ* example indicated sediment transport towards the northwest. All of the sandstone beds have sharp bases and tops. The bases of some beds have tool marks and poorly preserved flute/scour marks (Fig. 6b), while the upper surfaces commonly have small, disc shaped objects, which may be fragments of clay or microbial mat. Obvious scouring occurred during sandstone deposition, as the base of some beds incise through thin shale into the underlying sandstone (Fig. 6c). Some sandstone surfaces are ripple marked. Most of the fossils observed occur at the base of the sandstone beds, although one example was noted, in a 25 cm thick bed, of fossil material 7–10 cm above the base (Fig. 6d/e).

The overlying middle and upper parts of the Aar Member are dominated by shale with common limestone beds up to 1.35 m thick, but typically less than 30 cm thick, and minor, thin sandstone beds. Some of the limestone beds are massive, while others are strongly laminated, and a few have internal hummocky cross stratification. A number of limestone beds are abruptly overlain by planar laminated sandstone and some by hummocky cross-bedded sandstone, one bed of which cuts out a thin carbonate horizon (Fig. 7a). The limestone beds vary from olive-brown through tan to bright mustard-brown on weathered surfaces.

The thickest three to five limestone beds of the upper part of the Aar Member form distinctive topographic benches that can be followed regionally. The upper two of these are generally the most prominent. Twenty to twenty-six m above the base of the Aar Member is a conspicuous, laminated, reddish-yellow (ginger) coloured unit (LG) up to 1.2 m thick. This locally includes three limestone beds separated by very thin shale beds. Of these limestones, the upper bed in particular displays well-developed hummocky cross stratification (Fig. 7b). Three to 4.5 m above the top of the LG the uppermost, and most conspicuous of the benches is formed by the thickest limestone, a wavy-bedded, black and tan coloured unit (WBT) (Fig. 7c). This limestone bed also has locally developed ripple and hummocky cross-stratification and a brecciated upper surface (Fig. 7d/e).

4.1. Depositional environment

The Aar Member described here is interpreted as having been deposited on a subsiding continental margin during a major marine transgression (Johnson and Baldwin, 1986; Walker and Plint, 1992; Zecchin, 2007). It represents sediment accumulation during the transition from a braided, sandy, fluvial environment (Kliphoek Sandstone) to a fully marine, clear water environment, which facilitated carbonate deposition (Mooifontein Member). The initial, shale-dominant section was most likely subtidal and experienced occasional influxes of flood and/or storm-induced sand that produced thin, lens-shaped sheets in an otherwise mud-dominant setting. Sandstone beds within the Aar Member are irregularly distributed and much less common in the upper part of this unit. We interpret these as having also been deposited during storm-induced density flows, based on common basal scouring and tool marks, particularly on the base of some of the thicker beds. Some sand was reworked by storm waves, as indicated by the common occurrence of hummocky cross-stratification. Hummocky cross stratification

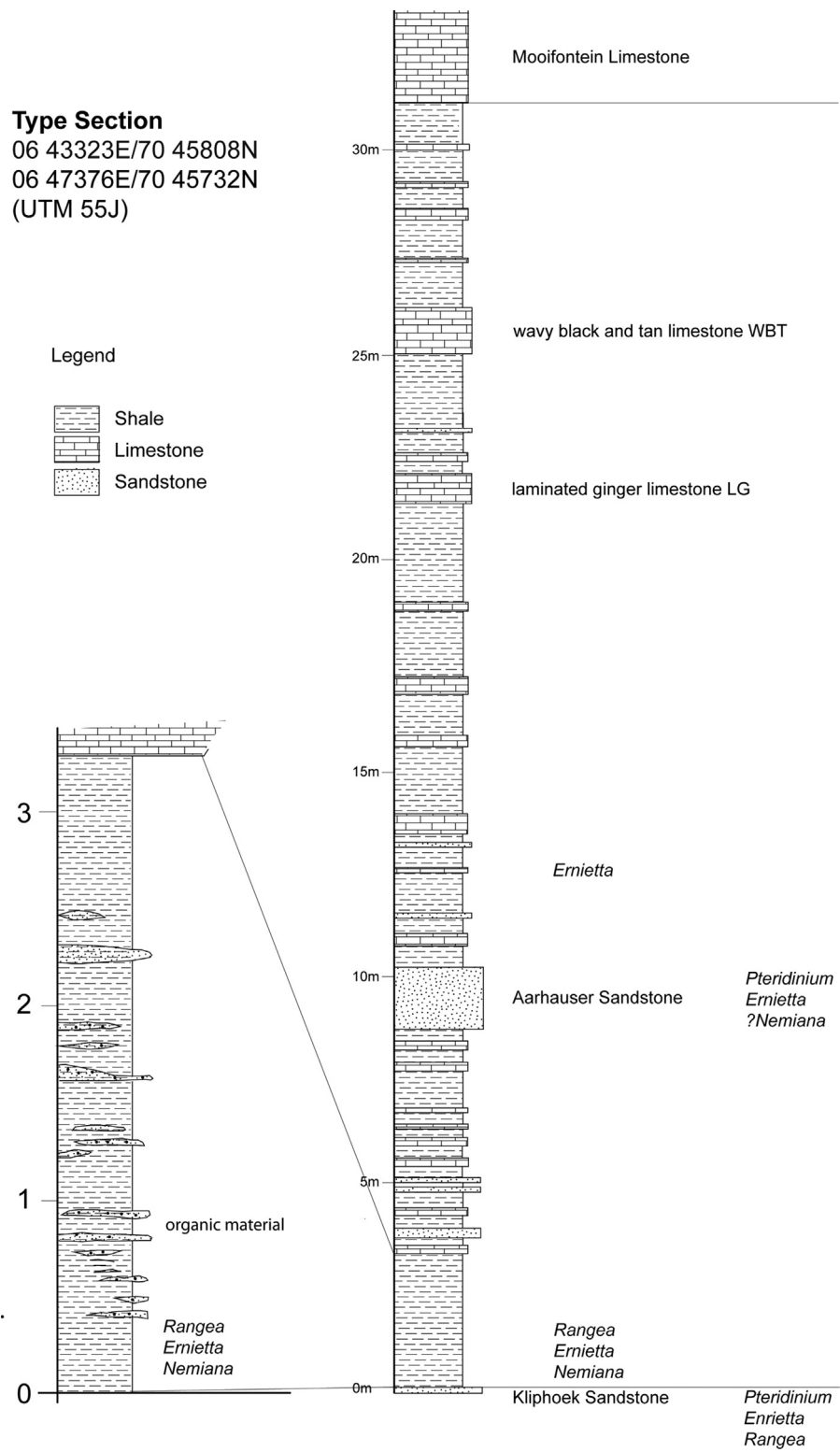


Fig. 4. Type Section of Aar Member, showing fossil locations.

within some of the thicker limestone beds and the brecciated upper surfaces again provide evidence of reworking by storm waves (see Fig. 7a/b).

The onset of limestone deposition reflects clearer, deeper water, isolated from clastic input, a result of the coastline moving craton-ward during an overall relative sea level rise. Carbonate deposition was periodically interrupted as a result of clastic (mud) build out

during relative sea level highstands or a slowing down in the rate of relative sea level rise, leading to interdigitations of carbonate and clastic sediments throughout the Aar Member. As the transgression continued, sea level finally rose to a level that prevented further clastic input and carbonate deposition prevailed. In sequence stratigraphic terms, the Aar Member can be viewed as an overall transgressive systems tract punctuated by shale-limestone

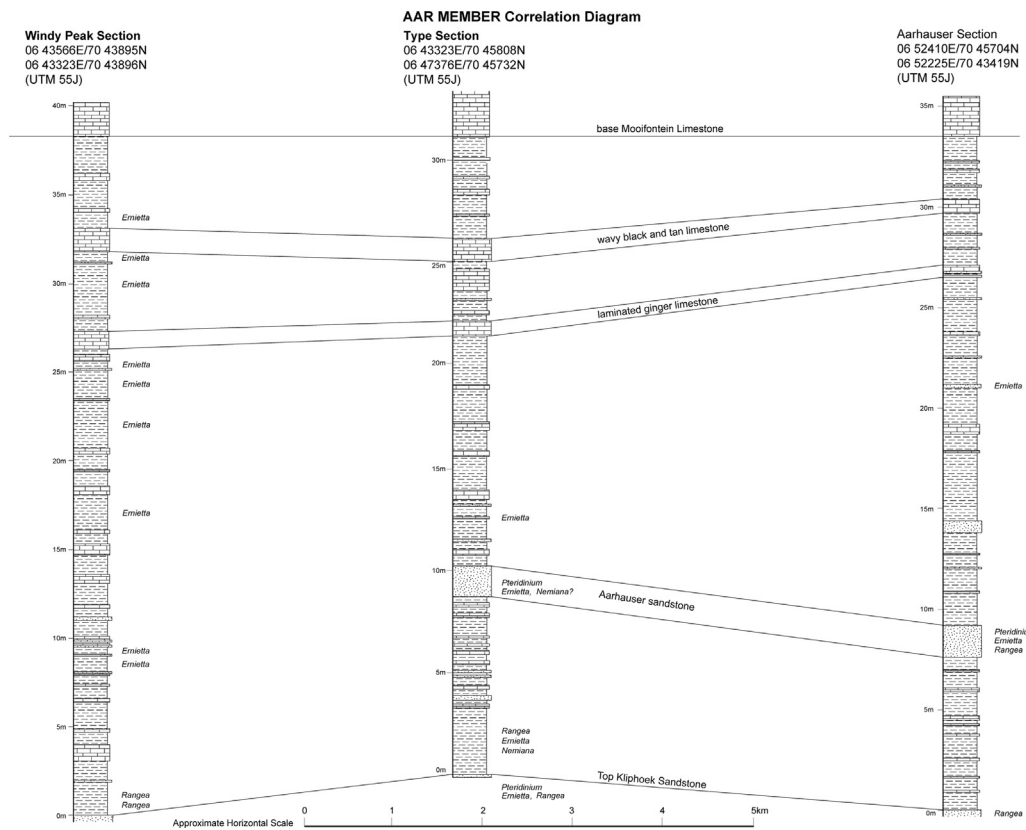


Fig. 5. Stratigraphic correlation diagram showing relationship between Type Section, Aarhauser and Windy Peak.

paracycles reflecting small-scale changes in relative sea level and sediment input over time.

4.2. Palaeontology

Fieldwork on Farm Aar from 2003 to 2011 involved several months of detailed investigation of the microenvironments that host the Ediacara organisms. Localities for each of the productive sites are recorded in the Geological Survey of Namibia catalogues in Windhoek. Ediacara taxa were recovered from a number of sedimentological settings, some transported and some preserved in life position. The following section covers each of these settings, and the accompanying detailed stratigraphic columns place each of these fossil assemblages within the stratigraphy of the Aar Member (see Figs. 4 and 5).

Pteridinium is most abundant in sediments at the top of the Kliphoek Sandstone and in the Aarhauser Sandstone in the lower part of the Aar Member (Elliott et al., 2011). Around the Type Section and in the Ernietta Hill area, 1–2 km east of Windy Peak, this taxon occurs at numerous localities within the uppermost 2 m of the Kliphoek Sandstone and is accompanied by *Ernietta* and rare *Rangea*. *Pteridinium* also occurs in an identical stratigraphic position at Aarhauser, where it is again associated with rare *Rangea*, and in valleys south of the Farm Aar homestead. The most abundant occurrences of *Pteridinium* are in the Aarhauser Sandstone at Aarhauser and along strike to the north and northwest, and at the Type Section of the Aar Member.

Ernietta is by far the most widespread and abundant fossil in the area, especially around Ernietta Hill, occurring at the top of the Kliphoek Sandstone and throughout the entire Aar Member. At the Type Section of the Aar Member, this taxon occurs in thin, lenticular sandstone beds in the basal 2–4 m of the member, while at Aarhauser large, brown *Ernietta* occur in a thin sandstone bed

12–13 m below the Mooifontein Member. In the Ernietta Hill area it occurs in a thin sandstone bed just above the top of the Kliphoek Sandstone, in sandstone beds in the lower third of the Aar Member at Ernietta Hill itself, where it is associated with *Nemiana*, and also in sandstone beds below the LG, between the LG and WBT, and between the WBT and base of the Mooifontein Member to the northeast, east and southeast of Ernietta Hill. At one locality ("Teapot") southeast of Ernietta Hill abundant, large, brown *Ernietta* specimens occur in a sandstone bed largely surrounded by faults, but probably stratigraphically below the LG.

In addition to the locations mentioned above, specimens of *Rangea*, associated with *Ernietta*, also occur in a thin sandstone bed just above the base of the Aar Member at the Type Section. Stromatolites are rare but were noted at the base of the Mooifontein Member limestone north of Aarhauser and in a mustard-yellow limestone bed in a faulted zone in the same area, but are probably from the upper part of the Aar Member. Finally, a few of the carbonate samples collected for the isotopic study contain occasional shelly fragments, potentially from *Cloudina*, and one that has clasts superficially similar to those interpreted as sponges (see Maloof et al., 2010).

4.3. Radiometric ages

To date no ash beds have been located in the Aar Member, but the unit does lie stratigraphically below an ash bed in what is considered elsewhere the uppermost Kuibis Subgroup and dated at 548.8 ± 1 Ma (Grotzinger et al., 1995), currently revised to 547.32 ± 0.31 (Narbonne et al., 2012). LA-ICP-MS U-Pb dating of detrital zircons (see Appendix 1 for method) from *Pteridinium*-bearing Aarhauser Sandstone at Aarhauser (Nam 125), summarized in Table 1, give concordia ages that range from ca. 2900 Ma to ca. 1100 Ma (Fig. 8), clearly reflecting the basement terrane from which

Table 1

U-Pb-Th isotope data used in construction of plot in Fig. 9.

Sample Numbers	$^{207}\text{Pb}^{\text{a}}$ (cps)	U^{b} (ppm)	Pb^{b} (ppm)	Th^{b} ^{206}Pb ^{204}Pb	$^{207}\text{Pb}^{\text{c}}$ ^{238}U	2σ %	$^{207}\text{Pb}^{\text{c}}$ ^{235}U	2σ %	$^{207}\text{Pb}^{\text{c}}$ ^{206}Pb	2σ %	rho^{d}	^{206}Pb ^{238}U	2σ (Ma)	^{207}Pb ^{235}U	2σ (Ma)	^{207}Pb ^{206}Pb	2σ (Ma)	conc %	
c37	7138	89	20	0.61	8346	0.19516	2.4	2.0108	4.0	0.07473	3.2	0.60	1149	25	1119	28	1061	65	108
c51	6477	43	9	0.59	8566	0.19061	2.7	1.9843	4.7	0.07550	3.8	0.58	1125	28	1110	32	1082	77	104
a1	4936	214	39	0.20	2460	0.17654	3.1	1.8431	4.1	0.07572	2.7	0.75	1048	30	1061	27	1088	55	96
c57	14,908	80	15	0.39	2717	0.17594	2.6	1.8381	4.9	0.07577	4.2	0.53	1045	25	1059	33	1089	84	96
c10	4307	48	10	0.46	5675	0.20061	2.5	2.0963	4.2	0.07579	3.4	0.58	1179	27	1148	29	1090	68	108
c54	5877	35	7	0.58	7774	0.18737	2.5	1.9589	5.0	0.07582	4.3	0.51	1107	26	1102	34	1090	86	102
a24	8783	329	64	0.16	6917	0.19577	3.6	2.0513	4.2	0.07600	2.2	0.85	1153	38	1133	29	1095	44	105
c53	3982	24	6	1.40	5226	0.18936	2.4	1.9862	4.4	0.07607	3.7	0.55	1118	25	1111	30	1097	74	102
c49	15,200	106	21	0.30	19,711	0.18752	2.4	1.9802	3.8	0.07659	2.9	0.65	1108	25	1109	26	1110	57	100
a37	11,485	436	84	0.46	15,133	0.17578	3.7	1.8581	4.2	0.07667	2.0	0.88	1044	35	1066	28	1113	40	94
a46	9528	197	42	0.39	12,491	0.20004	3.2	2.1242	4.0	0.07701	2.4	0.80	1176	34	1157	28	1122	48	105
b28	5900	78	15	0.46	7552	0.17491	3.4	1.8583	6.1	0.07706	5.1	0.55	1039	32	1066	41	1123	102	93
b30	11,742	153	32	0.38	14,883	0.19701	3.5	2.1034	4.1	0.07743	2.3	0.84	1159	37	1150	29	1132	45	102
a55	11,164	161	31	0.33	14,530	0.18369	3.7	1.9642	4.6	0.07755	2.7	0.81	1087	37	1103	31	1135	54	96
a52	4576	74	16	0.67	3445	0.19290	3.7	2.0677	5.8	0.07774	4.5	0.63	1137	38	1138	41	1140	90	100
a40	3217	96	21	0.78	4113	0.17922	3.7	1.9261	6.0	0.07795	4.7	0.62	1063	37	1090	41	1146	93	93
c3	6024	68	17	1.53	2192	0.18343	2.7	1.9726	3.7	0.07800	2.5	0.72	1086	27	1106	25	1147	50	95
a49	6657	119	24	0.36	8623	0.19436	3.8	2.0913	4.9	0.07804	3.2	0.76	1145	40	1146	34	1148	63	100
a39	1791	57	14	1.32	2307	0.17552	3.8	1.8912	6.0	0.07815	4.7	0.63	1042	37	1078	41	1151	93	91
a34	7791	303	62	0.63	10,047	0.17451	3.5	1.8844	4.8	0.07832	3.2	0.74	1037	34	1076	32	1155	64	90
b19	10,363	112	24	0.28	13,195	0.20865	3.2	2.2588	4.3	0.07852	2.9	0.74	1222	36	1200	31	1160	58	105
b15	12,213	135	25	0.32	2753	0.18139	3.7	1.9683	4.3	0.07870	2.1	0.87	1075	37	1105	29	1165	42	92
a42	7115	186	38	0.42	9111	0.18820	3.6	2.0492	4.9	0.07897	3.4	0.73	1112	37	1132	34	1171	66	95
a44	4444	106	24	0.89	5668	0.17969	3.9	1.9605	6.0	0.07913	4.6	0.65	1065	38	1102	41	1175	91	91
a19	12,124	413	78	0.12	14,281	0.19347	3.9	2.1254	5.3	0.07968	3.6	0.73	1140	40	1157	37	1189	70	96
c21	1512	16	4	0.90	1887	0.21906	4.4	2.4107	7.8	0.07981	6.4	0.57	1277	51	1246	58	1192	127	107
a43	6063	136	30	0.51	7644	0.19892	3.4	2.1962	4.9	0.08008	3.5	0.69	1170	36	1180	35	1199	70	98
a13	9538	333	68	0.31	12,022	0.19933	3.7	2.2014	5.0	0.08010	3.4	0.73	1172	40	1181	36	1199	68	98
a29	17191	631	133	0.50	21681	0.19026	3.6	2.1013	4.2	0.08010	2.2	0.86	1123	37	1149	29	1199	43	94
a25	11389	404	102	1.03	14319	0.20944	3.4	2.3210	4.8	0.08037	3.3	0.72	1226	38	1219	34	1206	65	102
a48	12317	235	46	0.56	15410	0.18362	4.2	2.0429	4.8	0.08069	2.3	0.88	1087	42	1130	33	1214	45	90
a31	1091	35	8	0.56	1351	0.19734	5.1	2.2033	7.6	0.08098	5.7	0.67	1161	54	1182	55	1221	112	95
a7	8468	350	72	0.45	5540	0.19194	5.2	2.1538	6.1	0.08139	3.2	0.85	1132	54	1166	43	1231	63	92
b9	8216	85	17	0.29	10039	0.19523	3.2	2.2022	4.2	0.08181	2.7	0.77	1150	34	1182	30	1241	52	93
a9	463	16	3	0.07	562	0.19671	5.7	2.2433	11.0	0.08271	9.4	0.52	1158	61	1195	80	1262	183	92
a41	18,324	476	111	0.47	22,375	0.21485	3.4	2.4520	5.0	0.08277	3.6	0.69	1255	39	1258	37	1264	71	99
a10	10,350	335	80	0.54	12,518	0.21485	3.3	2.4780	4.1	0.08365	2.4	0.80	1255	38	1266	30	1284	47	98
c11	14,269	134	31	0.39	16,360	0.21889	3.2	2.5716	4.1	0.08521	2.6	0.78	1276	38	1293	31	1320	50	97
c9	13,281	111	27	0.73	2399	0.20804	2.4	2.4649	4.2	0.08593	3.4	0.58	1218	27	1262	31	1337	66	91
c14	14,574	140	35	0.86	15,055	0.21276	2.6	2.5240	3.1	0.08604	1.7	0.83	1243	29	1279	23	1339	33	93
c25	17,896	157	46	0.64	20,759	0.25521	2.4	3.0299	2.9	0.08611	1.6	0.83	1465	31	1415	22	1341	31	109
a23	19,682	597	142	0.55	4438	0.21703	4.0	2.5799	4.3	0.08622	1.6	0.93	1266	46	1295	32	1343	30	94
b2	5833	51	13	0.54	5612	0.23249	2.9	2.7666	3.9	0.08630	2.7	0.73	1348	35	1347	30	1345	52	100
c7	22,673	186	51	0.55	26,344	0.23818	2.3	2.8407	3.0	0.08650	2.0	0.76	1377	28	1366	23	1349	38	102
b1	6066	65	17	0.76	4330	0.23275	4.8	2.7931	6.3	0.08704	4.0	0.77	1349	59	1354	48	1361	77	99
a28	23,792	713	176	0.61	12,908	0.21820	3.7	2.6441	4.2	0.08788	2.0	0.88	1272	43	1313	31	1380	38	92
b13	1961	17	4	0.41	2231	0.24045	3.3	2.9229	7.1	0.08816	6.3	0.46	1389	41	1388	55	1386	121	100
a32	9271	277	66	0.45	10,587	0.22309	3.3	2.7245	4.4	0.08858	2.9	0.75	1298	39	1335	33	1395	56	93
c27	18,591	155	43	0.53	19,970	0.24976	2.8	3.2139	3.7	0.09333	2.5	0.74	1437	36	1461	29	1494	47	96
b6	5421	31	12	1.05	5238	0.29179	3.0	4.1187	4.8	0.10237	3.8	0.62	1650	44	1658	40	1668	70	99
a14	17,304	318	99	0.38	9011	0.28583	3.5	4.0987	4.3	0.10400	2.5	0.82	1621	51	1654	36	1697	46	96
c32	27,220	161	59	0.94	4699	0.30003	2.3	4.3767	3.3	0.10580	2.3	0.71	1691	35	1708	28	1728	43	98
a8	16536	344	116	1.06	15,510	0.30005	3.4	4.4431	4.3	0.10740	2.6	0.80	1692	51	1720	36	1756	47	96
c17	40321	185	68	0.36	35184	0.33681	2.5	5.2655	2.8	0.11338	1.2	0.90	1871	41	1863	24	1854	22	101
c30	18109	84	35	0.46	15,860	0.37501	2.8	5.8977	3.9	0.11406	2.7	0.72	2053	49	1961	34	1865	48	110
a15	9192	138	60	1.02	6416	0.33449	3.2	5.3027	4.3	0.11498	2.8	0.75	1860	52	1869	37	1880	51	99
a27	19290	274	122	0.81	11,715	0.36503	3.5	5.8289	4.2	0.11581	2.3	0.84							

Table 1 (Continued)

Sample Numbers	$^{207}\text{Pb}^{\text{a}}$ (cps)	U ^b (ppm)	Pb ^b (ppm)	Th/U	^{206}Pb / ^{204}Pb	^{207}Pb / ^{238}U	2σ %	^{207}Pb / ^{235}U	2σ %	^{207}Pb / ^{206}Pb	2σ %	$\rho_{\text{ho}}^{\text{d}}$	^{206}Pb / ^{238}U	2σ (Ma)	^{207}Pb / ^{235}U	2σ (Ma)	^{207}Pb / ^{206}Pb	2σ (Ma)	conc %
b14	33,721	85	44	0.50	20,878	0.44138	3.4	9.8315	3.8	0.16155	1.7	0.90	2357	68	2419	36	2472	28	95
a6	20,225	123	90	1.21	11,433	0.50968	3.9	12.5605	4.7	0.17874	2.7	0.82	2655	85	2647	46	2641	45	101
a58	38,893	71	43	0.52	20,796	0.50620	3.4	13.1725	3.7	0.18873	1.3	0.93	2640	75	2692	35	2731	22	97
a51	89085	208	123	0.44	30,854	0.51838	3.7	14.7862	4.0	0.20687	1.5	0.92	2692	82	2802	39	2881	25	93

^a Within-run background-corrected mean ^{207}Pb signal in counts per second.^b U and Pb content and Th/U ratio were calculated relative to GJ-1 and are accurate to approximately 10%.^c Corrected for background, mass bias, laser induced U-Pb fractionation and common Pb (if detectable, see analytical method) using Stacey and Kramers (1975) model Pb composition. $^{207}\text{Pb}/^{235}\text{U}$ calculated using $^{207}\text{Pb}/^{206}\text{Pb}/(^{238}\text{U}/^{206}\text{Pb} \times 1/137.88)$. Errors are propagated by quadratic addition of within-run errors (2SE) and the reproducibility of GJ-1 (2SD).^d Rho is the error correlation defined as $\text{err}^{206}\text{Pb}/^{238}\text{U}/\text{err}^{207}\text{Pb}/^{235}\text{U}$.

the sand was derived. Two basement samples (Nam 66 and 67) from southwest of Farm Aar homestead, collected from just below unconformably overlying Nama Group sediments, give concordia ages of 1985 ± 10 Ma and 1989 ± 12 Ma, respectively (Fig. 9a/b). All zircons appear to be derived from the basement of the underlying Kalahari Craton. No addition of any debris derived from a younger, Neoproterozoic magmatic source is traceable.

5. Chemostratigraphy

5.1. Sample descriptions

A total of 66 limestone and siliciclastic samples were collected from the Aarhauser, Type Section, and Windy Peak sections (Figs. 10–12; Table 2). In addition, at the Windy Peak section, nine



Fig. 6. Detail of sandstone beds in Aar Member. (a) Thin sandstone beds interbedded with shale, basal part of Aar Member; Type Section. (b) Scour casts on base of sandstone bed, Aarhauser Sandstone; Aarhauser. (c) Detail of bedding within Aarhauser sandstone; Aarhauser. (d) *Pteridinium* preserved on base (sole) of a sandstone bed, Aarhauser Sandstone; Aarhauser. (e) Fragments of *Pteridinium* in lower part of a sandstone bed, Aarhauser Sandstone; Aarhauser.

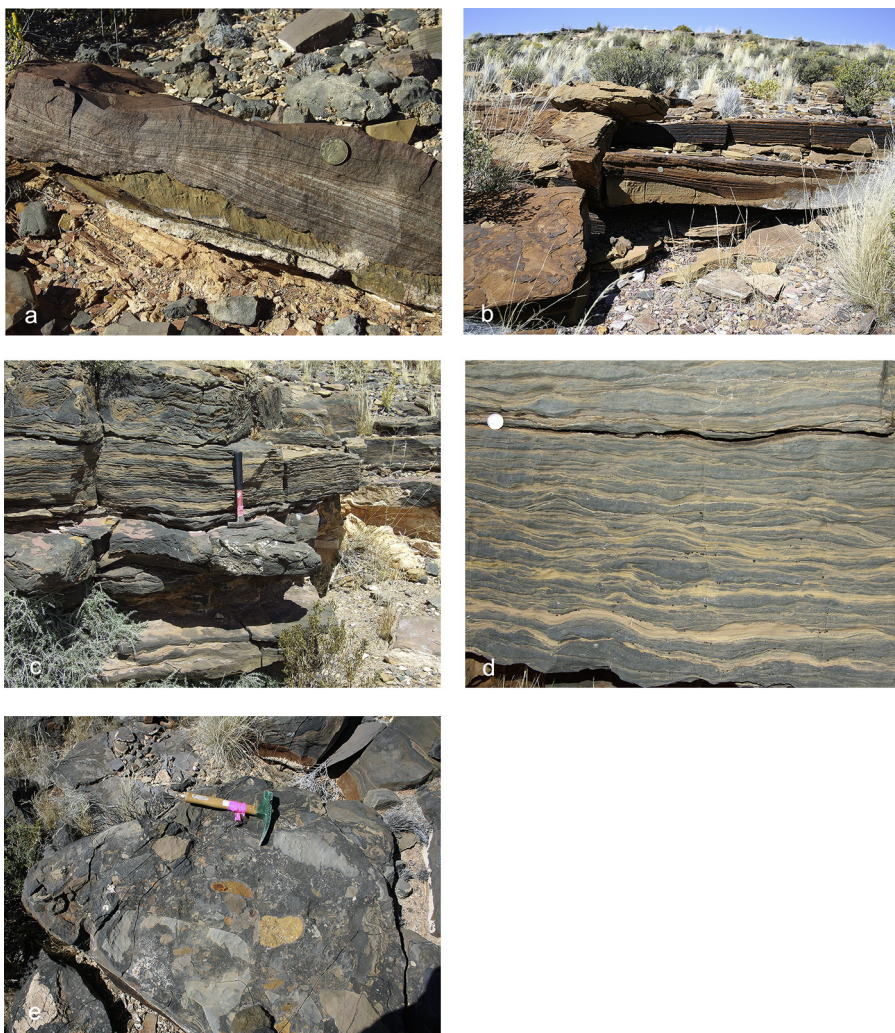


Fig. 7. Detail of bedding in carbonate units in Aar Member. (a) Hummocky cross-stratified sandstone bed overlying thin carbonate. Note irregular upper surface of the carbonate bed; North of Aarhauser. (b) Hummocky cross-stratification in laminated ginger (limestone) unit (LG); Windy Peak. (c) Typical wavy bedding in outcrop of wavy black and tan (limestone) unit (WBT); near Farm Aar homestead. (d) Ripple-like bedding in wavy black and tan (limestone) unit (WBT); Type Section. (e) Brecciated upper surface of wavy black and tan (limestone) unit (WBT); Windy Peak.

Nam 125, n=76/120, 90–110% conc.

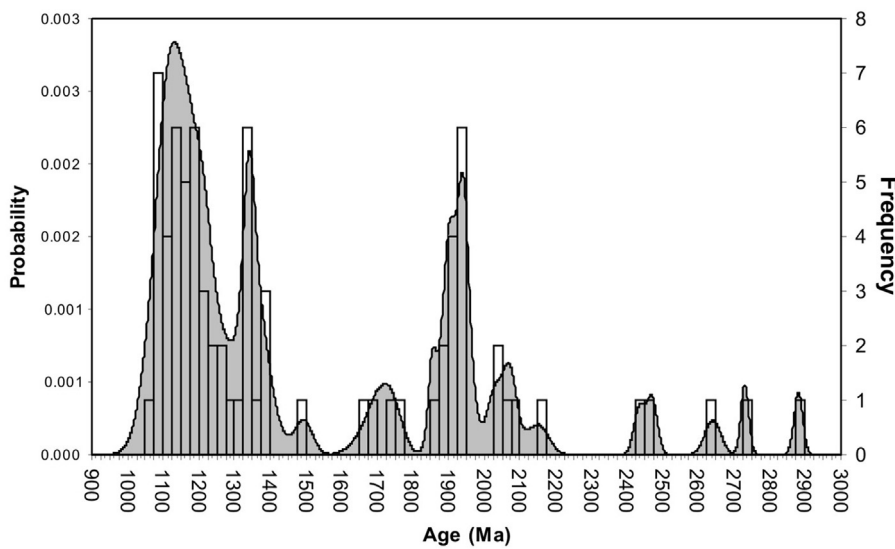


Fig. 8. Sample Nam 125; distribution of zircon ages in Aarhauser sandstone, Aarhauser.

Table 2

Descriptions and isotopic compositions of geochemical samples (Aar Member, Type, Aarhauser and Windy Peak sections) discussed in the text and/or used in Figs. 10–12.

Sample Numbers	Height (m)	Description	$\delta^{13}\text{C}$ (‰, VPDB)	$\delta^{18}\text{O}$ (‰, VPDB)	S (wt.%)	$\delta^{34}\text{S}$ (‰, VPDB)	$^{87}\text{Sr}/^{86}\text{Sr}$
<i>Aarhauser section</i>							
A1	3.7	Olive-brown massive lms	-2.65	-11.98			
A2	4.3	Laminated olive-brown lms					
A3	4.6	Massive to intraclastic/fossiliferous?	-3.57	-6.34			
		Olive-brown argillaceous lms					
A4	6.1	Laminated olive-brown to brown lms	-3.04	-6.94			
A5	7.0	Laminate light grey to brown lms	-4.05	-7.10			
A6	11.0	Massive variegated olive-brown argillaceous lms	-3.47	-4.47			
A7	12.9	Laminated peloidal olive-brown clastic lms	-2.51	-5.98			
A8	18.1	Laminate light grey to brown lms	-1.30	-6.73			0.72063
A9	19.2	Massive chocolate brown clastic lms	-1.66	-7.64			
A10	24.1	Massive chocolate-red lms	-1.40	-6.36			
A11	27.4	Massive red to brown mottled lms	-2.67	-7.08			
A12	28.4	Massive chocolate brown clastic lms	-1.61	-9.57			
A13	30.5	Laminated grey to olive-green lms with precipitates	0.83	-10.50			0.70923
A14	32.1	Massive chocolate-red lms	-0.87	-7.25			
A15	32.3	Massive variegated black to chocolate-red lms	2.84	-12.19	0.62	4.74	
A16	32.8	Massive variegated grey to brown lms	-0.89	-7.37			
A17	33.4	Laminated grey to brown sandstone					
A18	35.1	Laminated dark grey to red argillaceous lms	4.47	-10.75			
A25					0.08	27.90	
<i>Type section</i>							
Q1	3.4	Olive grey massive lms					
Q2	4.3	Laminated dark grey to brown lms	-4.37	-12.86	0.21	20.68	
Q3	5.5	Intraclastic olive grey to grey lms	-0.21	-12.36			
Q4	3.0	Mottled brown to grey argillaceous lms	-2.55	-6.16			
Q5	6.8	Massive brown argillaceous lms	-1.64	-5.74			
Q6	7.8	Laminated dark grey clastic lms	-1.47	-10.10			
Q7	8.3	Laminated dark grey to brown lms	-1.65	-10.35			
Q8	9.7	Laminated reddish grey sandstone					
Q9	10.8	Laminated dark grey to brown lms with precipitates	0.18	-10.53			0.70951
Q10	12.5	Laminated grey to brown clastic lms with precipitates	0.17	-10.81			0.70920
Q11	13.6	Laminated grey to brown argillaceous lms	0.08	-10.05			
Q12	15.6						
Q13	16.9	Mottled brown pisolithic lms	-0.89	-10.38			
Q14	18.8	Mottled chocolate brown pisolithic lms	-1.73	-6.36			
Q15	21.6	Mottled chocolate brown clastic lms	-1.73	-6.15			
Q16	22.3	Laminated olive grey intraclastic lms	1.66	-7.47			
Q17	23.0						
Q18	25.4	Laminated dark grey to reddish clastic lms	0.86	-10.00			
Q19	27.1	Red to brown pebble conglomerate					
Q20	28.2	Variegated red to brown intraclastic lms	-0.63	-7.53			
Q21	28.8	Intraclastic/fossiliferous? brown to grey lms	-0.59	-10.73			

Table 2 (Continued)

Sample Numbers	Height (m)	Description	$\delta^{13}\text{C}$ (‰, VPDB)	$\delta^{18}\text{O}$ (‰, VPDB)	S (wt.%)	$\delta^{34}\text{S}$ (‰, VPDB)	$^{87}\text{Sr}/^{86}\text{Sr}$
Q22	29.7	Laminated olive grey to grey clastic lms with fine grained reddish ash?	-1.20	-7.09			
Q23	32.0	Laminated dark grey to chocolate brown intraclastic/fossiliferous? lms	1.56	-8.85			
<i>Windy Peak section</i>							
W1	Below KL ss	Green matrix grit sandstone					
W2	Below KL ss	Massive light brown clastic lms					
W3	Below KL ss	Massive light grey recrystallized lms	-4.01	-13.90			
W4	Below KL ss	Massive light grey clastic lms	-5.91	-18.20			
W5	Below KL ss	Laminated light grey to brown carbonaceous sandstone	-5.47	-10.08			
W6	Below KL ss	Mottled buff sandstone					
W7	Below KL ss	Laminated light grey to brown carbonaceous sandstone	-5.02	-17.15			
W8	Below KL ss	Laminated dark grey clastic/recrystallized lms	-4.38	-10.15	0.94	-2.51	
W9	Below KL ss	Laminated light grey siltstone					
W10	3.3	Laminated chocolate brown argillaceous lms	-1.28	-6.49			
W11	3.9	Massive dark grey lms	-0.96	-13.75			
W12	4.8	Laminated dark grey to brown peloidal lms	-0.51	-12.95	0.11	10.88	
W13	6.6						
W14	7.7	Laminated dark grey intraclastic argillaceous lms	0.07	-12.07	0.17	24.35	
W15	8.1	Laminated dark grey argillaceous lms	-0.54	-11.04	0.19	23.76	
W16	9.8	Laminated dark grey argillaceous lms with precipitates	1.72	-10.16	0.30	26.68	0.71041
W17	10.1	Massive brown to grey recrystallized lms	-0.39	-12.91	0.35	10.98	
W18	11.9	Laminated grey to brown argillaceous lms	-0.64	-9.18			
W19	13.4	Massive dark grey argillaceous lms	1.94	-12.50	0.33	17.95	
W20	15.0		1.28	-12.90	0.24	16.77	
W21	15.3	Massive brown clastic lms	0.11	-6.71			
W22	16.2	Laminated grey to reddish brown intraclastic lms	1.78	-10.74	0.07	23.45	
W23	18.6	Massive grey to brown clastic lms	0.55	-11.51	0.18	33.26	
W24	19.6	Laminated olive grey lms with oxides	-2.72	-7.64			
W25	20.7	Laminated dark grey to brown clastic argillaceous lms	0.87	-11.02	0.19	23.70	
W26	26.0	Massive dark grey argillaceous lms	1.59	-10.48			
W27	26.4	Laminated dark grey argillaceous lms	2.76	-11.72	0.06	26.64	
W28	28.4	Laminated brown to grey argillaceous lms	3.36	-5.77	0.25	16.82	
W29	31.3	Laminated dark grey to chocolate red argillaceous lms	-0.23	-7.83	0.07	18.80	
W30	32.5	Massive intraclastic grey to brown argillaceous lms	0.67	-10.04	0.28	3.84	
W31	34.4	Massive variegated reddish brown calcareous ash?	0.70	-6.83			
W32	36.3	Red to grey calcareous ash?					
W33	37.6	Laminated light brown calcareous siltstone/ash? with oxides	-0.50	-8.45			
W34	40.5	Massive dark grey lms	2.41	-11.20			

samples were collected from an interbedded limestone and shale interval below the Kliphoek Sandstone. Limestones from these beds are significantly recrystallised and light grey in colour on fresh surfaces but distinctly dark green-grey when weathered, whereas those from beds above the Kliphoek Sandstone at this locality and elsewhere are typically clastic, fine- to medium-grained, grey to

olive-brown in colour, argillaceous, and laminated, suggesting a subtidal depositional environment. Notably, one sample from this section preserves neomorphosed aragonite crystal fans suggesting high carbonate alkalinity in shallow seawater.

Aragonite precipitation fabrics are also observed in two closely spaced samples at roughly the same stratigraphic horizon

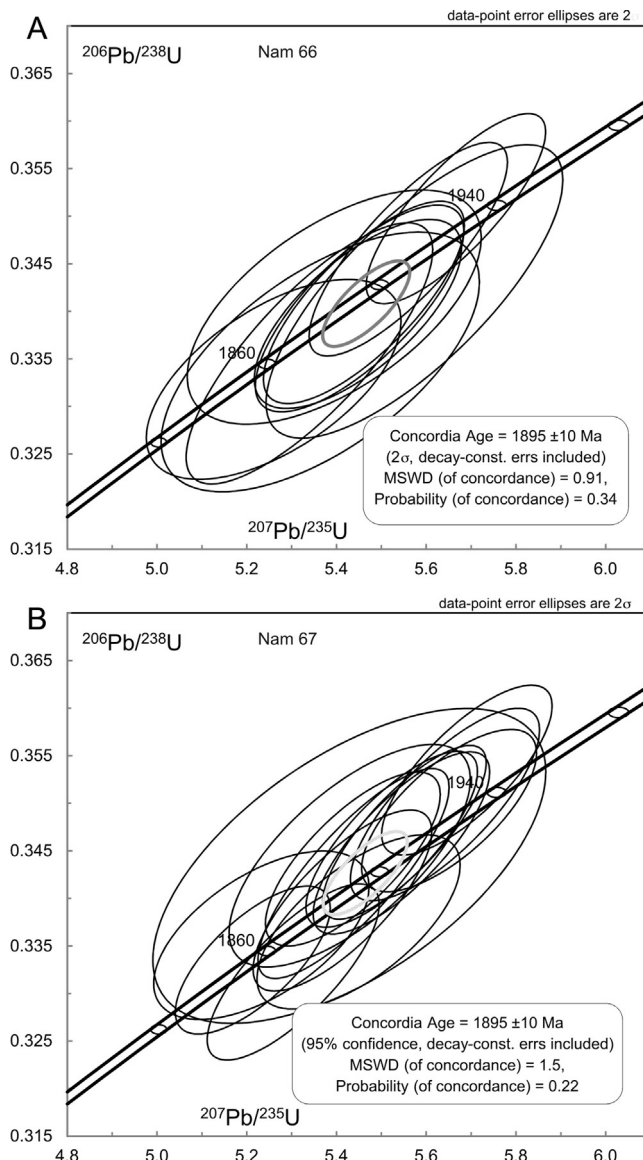


Fig. 9. Concordia ages. 11a, Sample Nam 66; basement sample, southwest of Farm Aar homestead. 11b, Sample Nam 67; basement sample, southwest of Farm Aar homestead.

represented at the Type Section. Most of the limestone samples from the Type Section are also fine- to medium-grained, grey to olive-brown in colour, argillaceous, and laminated; some of the samples are grainstones with intraclasts, pisoliths, and possible shelly fragments. Most of the limestone samples from the Aarhauser strata are massive to weakly laminated and olive-brown to yellowish in colour. None of these argillaceous, clastic limestones preserve aragonite pseudomorphs. Based on these lithostratigraphic observations, it seems possible that the transect from Aarhauser to Type Section to Windy Peak represents a proximal to distal sampling of the Aar Member.

Methods of geochemical analysis are described in Appendix 2.

5.2. Time-series geochemistry

Methods of geochemical analysis are described in Appendix 2 and the carbon and oxygen stable isotopic data are compiled in Table 2 and illustrated in Figs. 10–12. Recrystallised limestone samples from the Windy Peak section below the Kliphoek Sandstone, but not illustrated, have consistently negative $\delta^{13}\text{C}$ values near

−5‰ with $\delta^{18}\text{O}$ values that range widely from −10 to −18‰. Above the Kliphoek Sandstone, limestone samples from the Aar Member at Windy Peak reveal a slight enrichment in both ^{13}C and ^{18}O higher in the section, with slightly negative $\delta^{13}\text{C}$ values near the base of the unit, rising to moderately positive (up to ca. +3.5‰) values near the top. Most samples, however, have compositions near 0‰. A very similar negative-to-positive carbon isotope trend is recorded in the Type Section, but oxygen isotopes are slightly enriched in ^{18}O relative to their Windy Peak counterparts. At the Aarhauser section further southeast, the chemostratigraphy is notably different. There the negative-to-positive transition in ^{13}C values is more pronounced, with all of the lower Aar Member samples consistently depleted in ^{13}C . Notably, the limestone samples from Aarhauser, including samples with negative $\delta^{13}\text{C}$ values, are more enriched in ^{18}O than samples from the Type Section and Windy Peak.

5.3. Diagenesis vs. secular variation

Given the noted differences in both carbon and oxygen stable isotope compositions from the three sections of the Aar Member, it is likely that these surface rocks were altered to varying degrees through the interaction of meteoric and metamorphic fluids. The pre-Kliphoek Sandstone Mara Member carbonates sampled at Windy Peak differ significantly in grain size, preservation of sedimentary textures, and strongly negative carbon and oxygen isotope values relative to all other samples from this study. The carbon isotopic compositions of these older carbonates are remarkably similar to those from the Mara Member of the Dabis Formation near Swartkloofberg, some 75 kilometres south of Farm Aar (Kaufman et al., 1991; Saylor et al., 1998). Given scant evidence for coarse recrystallization in post-Kliphoek limestone samples, it is plausible that the pre-Kliphoek marble was affected by hydrothermal activity.

All other limestone samples from this study are fine-grained and preserve sedimentary textures, but given their wide range of $\delta^{18}\text{O}$ values it is likely that most samples have been altered to some degree by meteoric fluids. Strontium isotope compositions of carbonate samples containing aragonite pseudomorphs are no lower than 0.7092 (Table 2), which is higher than predicted for this time interval (Kaufman et al., 1993; Halverson et al., 2007) and is likely the result of radiogenic ingrowth of ^{87}Sr from Rb in intermixed clays. However, even if meteoric fluids did pass through these carbonates, they do not appear to have been laden with carbon from a terrestrial source, insofar as most analyses lie outside of the diagenetic stabilization trend defined for Neoproterozoic carbonates (Knauth and Kennedy, 2009). In fact, the Aar Member samples (in the lower part of the Aarhauser section) most depleted in ^{13}C show the greatest enrichment in ^{18}O within the sample set. Thus, the negative-to-positive up section $\delta^{13}\text{C}$ trends revealed in each of the three Aar Member sections are interpreted as true secular variations. These time-series trends are consistent with earlier low-resolution studies that show a strong negative-to-positive excursion across the K1/K2 depositional sequences (Kaufman et al., 1991; Saylor et al., 1998).

The more pronounced excursion in the Aarhauser section reflects the more strongly ^{13}C depleted limestone samples from this locality relative to those at Aar Member Type Section and Windy Peak. While these might reflect small differences in the carbon stable isotopic compositions of proximal vs. distal water masses (see Corsetti and Kaufman, 2003), this contrast could also indicate diachroneity of sediment accumulation across the platform, or of missing section in the Aarhauser locality. In either case, it appears that the Ediacaran taxa discovered in the Aar Member ($>547.32 \pm 0.31$ Ma) survived and diversified at a time of significant change in the carbon isotopic composition of seawater. In

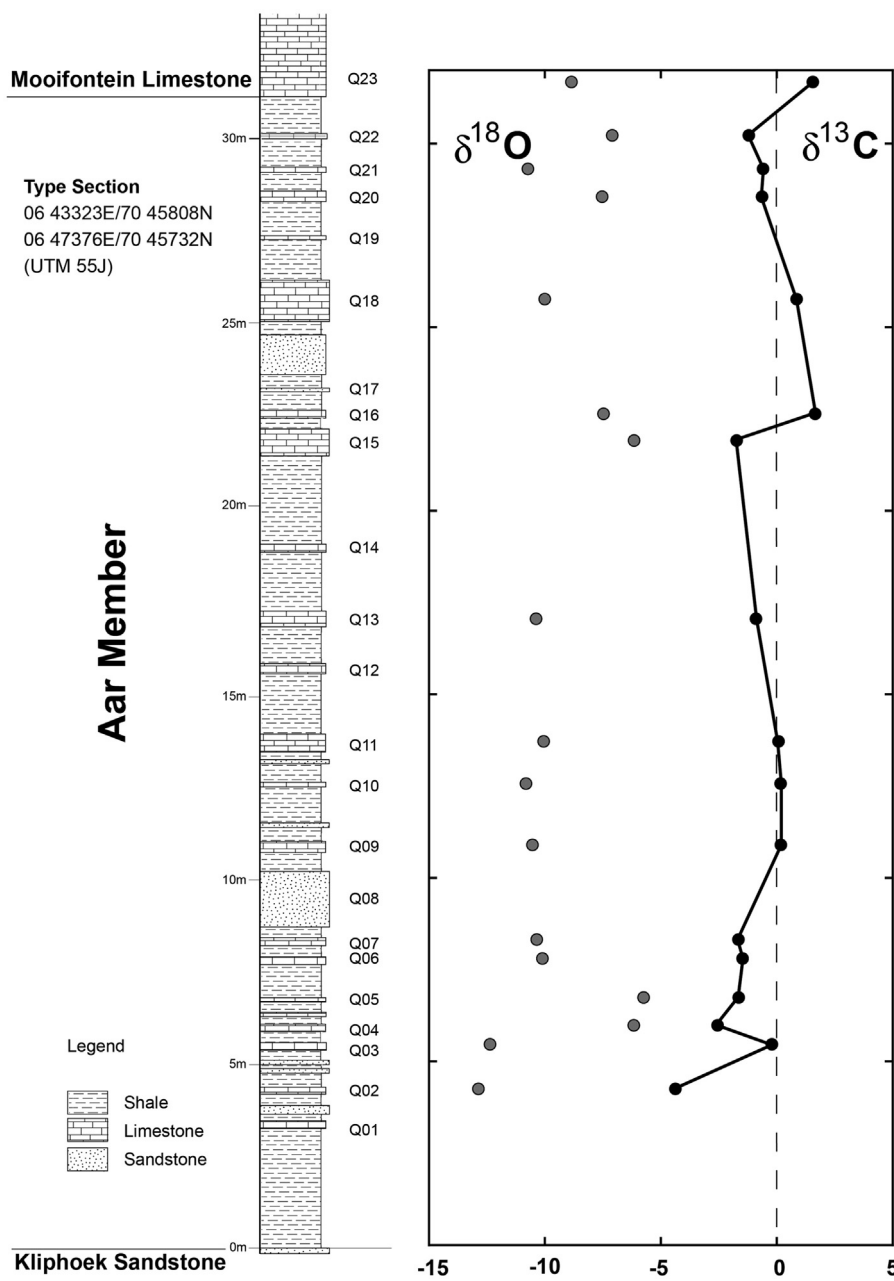


Fig. 10. $\delta^{18}\text{O}$ and $\delta^{13}\text{C}$ geochemistry; Aar Member, Type Section.

addition, *Cloudia* occurs in limestone of the underlying Mara Formation, which preserves strongly negative $\delta^{13}\text{C}$ values (Kaufman et al., 1991; Saylor et al., 1998; Grotzinger and Miller, 2008) that are potentially correlative with a profound negative carbon isotope anomaly (with $\delta^{13}\text{C}$ values as low as $-12\text{\textperthousand}$) known as the Shuram event in middle Ediacaran successions worldwide.

6. Taphonomy

Detailed morphological preservation of some of the fossils in the Aar Member appears to be the result of pyritization of the decomposing organism (Vickers-Rich et al., 2013). Evidence for an original pyrite “death mask” for some of the *Rangea* fossils preserved near the base of the member comes from the discovery of a fine-grained yellow mineral crust on the surface of the trace fossils. Mineral components of the yellow crust were identified using powder X-ray

diffraction. A small quantity of a representative crust was scraped from the surface of a fossil and ground under anhydrous ethanol to produce a slurry, which was mounted and dried on a glass slide at room temperature. Qualitative mineral identification was done using a Bruker D8 θ - 2θ X-ray diffractometer equipped with a scintillation detector in the School of Chemistry, Monash University. A long, fine-focus Cu X-ray tube was operated at 40 kV and 40 mA. Data for mineral identification were collected with a step size of 0.02° 2θ and counting time of 2 s/step over a range of 2 – 80° 2θ . Constituent mineral phases were identified with reference to the ICDD PDF-2 database using the software programme DIFFRAC^{plus} EVA.

The most abundant mineral component of the yellow crust sample was quartz, which was accompanied by moderate amounts of muscovite and biotite, and most notably by minor abundances of jarosite [nominally $\text{KFe}^{3+}_3(\text{SO}_4)_2(\text{OH})_6$] and kaolinite. The

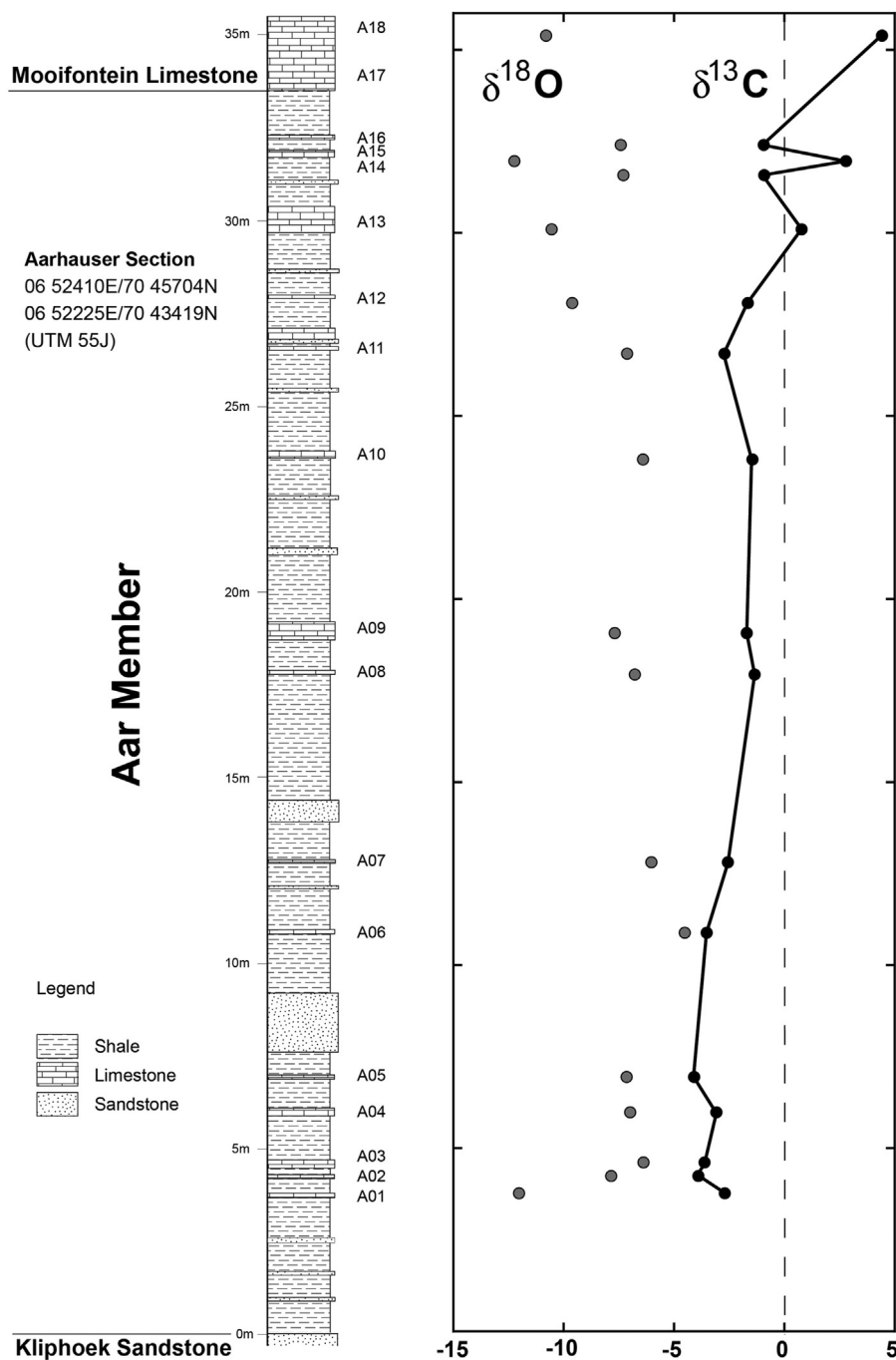


Fig. 11. $\delta^{18}\text{O}$ and $\delta^{13}\text{C}$ geochemistry; Aar Member, Aarhauser section.

sulphur content of the yellow crust scraped from sample FG32B was quantified with a Eurovector elemental analyzer to be $\sim 6.5\%$. This jarosite is likely to have formed during oxidative weathering of pyrite (Jambor and Blowes, 1998; Lottermoser, 2010) in the presence of K-bearing silicate minerals such as micas and K-feldspars (Bladh, 1982). Oxidative weathering of pyrite commonly produces sulphuric acid and Fe-oxide and oxyhydroxide phases, such as hematite and goethite (Jambor and Blowes, 1998; Lottermoser, 2010). This process can also produce jarosite when K is leached from K-bearing silicate minerals during acid weathering (Bladh, 1982). Muscovite and biotite, present at moderate abundances, would be subject to acid leaching as a consequence of this reaction, which would provide a source of K for jarosite. Furthermore, kaolinite commonly forms under Earth-surface conditions by weathering of

K-feldspar and muscovite in mildly acidic rainwater and surface waters (Murray, 1988). The presence of both kaolinite and jarosite in the sample suggests the formation of these minerals is connected to oxidative weathering of pyrite.

Supporting this interpretation, the sulphur isotope composition of the jarosite crust was determined to be $\sim +26.6\text{\textperthousand}$, which is consistent with the highly enriched ^{34}S abundances of pyrite in bulk samples throughout the Aar Member (Table 2). It has previously been suggested that pyritization of the Ediacara organisms co-occurring with microbial mats was an important factor in the unusual modes of preservation of these soft-bodied organisms (Gehling, 1999). Our discovery of jarosite on the surface of some of the Aar Member specimens supports this hypothesis insofar as the oxidative product represents a mineralogical vestige of

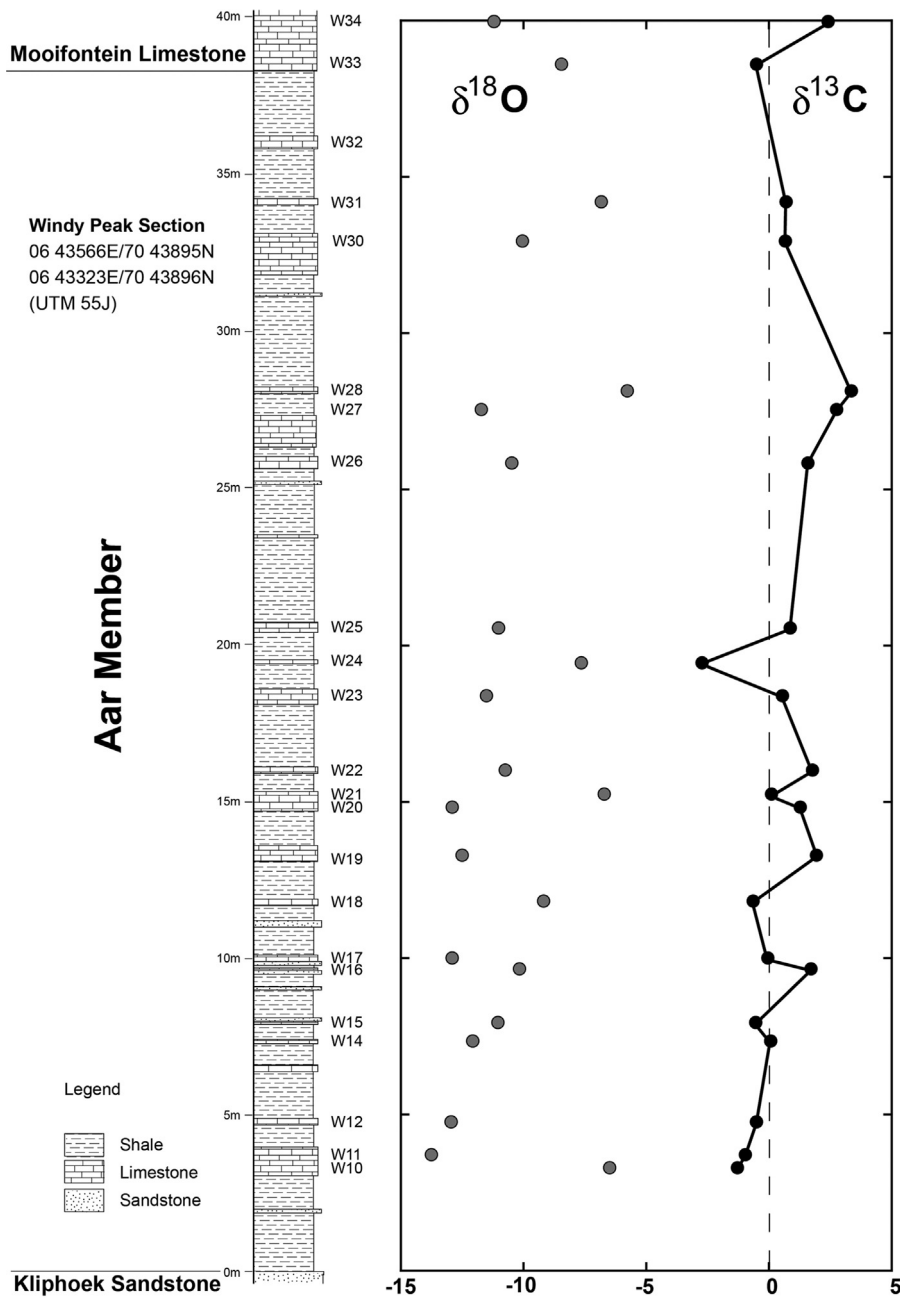


Fig. 12. $\delta^{18}\text{O}$ and $\delta^{13}\text{C}$ geochemistry; Aar Member, Windy Peak section.

pre-existing pyrite and further opens the taphonomic window to fossils entombed in sandstone.

7. Redox and the Ediacara biota

In the “death mask” model, pyritization of a decomposing metazoan would stabilize its surface (as well as some internal morphologic details) and allow the external form of the organism to be imprinted with exquisite detail on fine-grained siliciclastic substrates. Insofar as bacteria that reduce sulfate by oxidation of simple organic substrates are obligate anaerobes, the death mask must have developed rapidly in anoxic pore waters where product HS^- was fixed with soluble Fe^{2+} into highly insoluble pyrite.

While anoxia may have been local and directly associated with the decomposition of *Rangea* organic matter by sulfate reducing bacteria, the source of the reactive ferrous iron remains problematic. Given that the sandy sediments are generally lacking in iron,

the most likely source of this element would be deep subtidal seawater, which would require anoxic conditions for iron to be soluble and mobile. The negative carbon isotope compositions of carbonates (interpreted as reflecting depositional rather than diagenetic conditions) interbedded with the fossiliferous sandstones (including the strongly negative $\delta^{13}\text{C}$ values of the underlying Mara Member, which includes *Cloudina*) support the view that subtidal seawater in the Nama Basin may have also been lacking in oxygen. Negative $\delta^{13}\text{C}$ values in carbonates are typically interpreted to reflect periods when proportionally less reduced organic matter was sequestered in sediments (Hayes, 1983) in response to either lower rates of primary productivity or of enhanced rates of aerobic mineralization (cf. McFadden et al., 2008 for an example from the Shuram event preserved in Ediacaran strata of south China), either of which would deplete oxygen from the water column. Independent evidence for anoxia during negative $\delta^{13}\text{C}$ excursions is recorded as trace metal and Ce/Ce^* anomalies in

carbonates (Kimura and Watanabe, 2001; Schröder and Grotzinger, 2007; Ling et al., 2013); conversely positive $\delta^{13}\text{C}$ anomalies are correlated with enrichments in ^{54}Cr in carbonates that have been linked to enhanced oxidation of surface environments (Frei et al., 2009, 2011). In our next field season we plan to sample through shale facies for subsequent Fe-speciation analyses to further test the anoxia hypothesis. Notably, both *in situ* *Ernietta* and transported *Pteridinium* and *Rangea* in the Aar Member are preserved in sandstone interbedded with limestone with negative $\delta^{13}\text{C}$ compositions.

The observation that the oldest Ediacara biota in Namibia (including *Cloudina* in the Mara Formation) is found in strata that record a strong negative-to-positive carbon isotope anomaly suggests that these organisms originated and diversified worldwide during rapidly changing environmental conditions. Specifically, *Ernietta* may have been tolerant of episodically or wholly anoxic conditions given its apparent *in situ* position on the marine platform. On the other hand, *Pteridinium* and *Rangea* more likely proliferated in more proximal oxygenated environments, but were transported and pyritized in deeper ferruginous settings.

Environmental variability through this Ediacaran Period is similarly recorded in the abundance and sulphur isotopic compositions of sulphides and trace sulphate in carbonates. The very low concentrations of sulphur and significant enrichment of ^{34}S in pyrite in many of the Aar Member samples (Table 2) are similar to those observed in “superheavy” pyrite recorded throughout the Nama Group and in other late Ediacaran successions. These unusual pyrites have been interpreted as the result of low oceanic sulphate concentrations coupled with either biological or abiological oxidation of sedimentary or aqueous sulphide in bottom waters during storm ventilation (Ries et al., 2009), or of strongly stratified water columns with low, but ^{34}S enriched, sulphate in bottom waters or a sulphate minimum zone (Shen et al., 2008). Notably superheavy pyrite is not ubiquitous in all Ediacaran ocean basins (Fike et al., 2006; Canfield et al., 2007), and iron-speciation results from a broadly equivalent and fossiliferous section in Newfoundland suggests that the deep Ediacaran ocean may have been oxygenated (Canfield et al., 2007). The contradictory data suggest that the redox characteristics of each of these basins may be unique, depending on local tectonic, oceanographic, and biological conditions.

The speculation that subtidal Nama Basin seawater was anoxic or sub-oxic may not greatly impact our understanding of the lifestyle of *Rangea* and *Pteridinium* insofar as these specimens were transported from their *in situ* position during storm events. Other Ediacara fossils (i.e., *Ernietta*) in the Aar Member, however, appear to be preserved in place (Vickers-Rich et al., 2013), and these metazoans (as well as *Cloudina* in the underlying Mara Member) may have evolved the capacity to survive under episodically toxic environmental conditions. Taphonomic preservation of the soft-bodied organisms would have been promoted by their rapid burial beneath an anoxic and ferruginous water column. Finally, mineral sulfide oxidation by bacteria could have played a role in the production of jarosite.

One other possibility for the transported assemblages may be that they were living in estuarine or even fluvial, better oxygenated environments and were introduced into the more anoxic environs where they were preserved. But, in the case of many clearly *in situ* *Ernietta* assemblages, this is not the case.

8. Conclusions

The newly defined and described Aar Member of the Nama Group, exposed on Farm Aar in southwest Namibia, hosts some of the youngest Ediacaran metazoans preserved globally. In the

past few years this unit has yielded a rich collection of fossils as detailed geological mapping has progressively refined both regional and local stratigraphy. The sequence represents a transition from fluvial to shallow marine environments, with the last of the Ediacarans preserved primarily in storm, flood-induced sands, rapidly deposited in an otherwise mud-dominated, offshore environment. Concentrations of *Pteridinium* appear to be transported, while some *Ernietta* assemblages are close to *in situ*. *Rangea* material has also been transported and is confined to thin sandstone lenses representing gutters in a near shore setting, clearly not far from where these early metazoans once lived. Some fossils are encrusted with the iron-sulfate mineral jarosite, which is similar in isotopic composition to pyrite that occurs throughout the member; these observations lend credence to the pyrite “death mask” hypothesis (Gehling, 1999).

Because of the uniqueness of what was once considered a single member of the Dabis Formation, we have sub-divided the Kliphoek Member into the (lower) Kliphoek Sandstone Member and the (upper) Aar Member, based on a type section and reference sections on Farm Aar, ESE of the town of Aus. The Aar Member is dominated by shale, but limestone beds become increasingly common higher in the stratigraphy, clearly reflecting transgression onto a subsiding continental margin.

Time-series carbon isotope trends through the Aar Member define the rising limb of a strong positive excursion coincident with ^{34}S enriched pyrite and the first appearance of the Ediacara biota in Namibia. Negative carbon isotope compositions plausibly reflect the oxidation of a large deep DOC (dissolved organic carbon) pool (McFadden et al., 2008), and low sulphur abundances and positive $\delta^{34}\text{S}$ values likely indicate low abundances of seawater sulphate. Together these observations support the view that subtidal environments were episodically anoxic. Such conditions would promote bacterial sulphate reduction and the production of pyrite “death masks” for the Ediacara biota. The rise in carbon isotope compositions through this interval suggests that shallow oceans became progressively oxygenated in the aftermath of the Shuram event, but fluctuations in seawater redox through the transitional interval support the view that some of the earliest metazoans may have evolved the capacity to survive under episodically anoxic environmental conditions, or were transported into them and there exquisitely preserved.

Acknowledgements

Thanks to Patricia Komarower for editorial assistance and to Draga Gelt for drafting assistance; Barbara Boehm-Ern and the late Bruno Boehm for their gracious hospitality and support on Farm Aar; C. Wimmers, M. Meyer, N. Fournie for assistance in collecting samples from the measured sections; the Waterhouse Club from Adelaide for their field assistance; Benjamin Breeden, Michael Conlon and Irene Kadel-Harder who assisted Kaufman with geochemical analyses at the University of Maryland. Thanks also to our respective institutions, to the National Geographic Society and the UNESCO International Geosciences Programme (IGCP587) and the Namibian Geological Survey for their assistance in so many ways. Guy Narbonne provided insightful discussion in the field and in the laboratory.

Appendix 1.

A.1. Radiometric analysis

Zircon concentrate was separated from 2 to 4 kg sample material at the Museum für Mineralogie und Geologie (Senckenberg Naturhistorische Sammlungen Dresden) using standard

methods. Final selection of the zircon grains for U-Pb dating was achieved by hand-picking under a binocular microscope. Zircon grains of all grain sizes and morphological types were selected, mounted in resin blocks and polished to half their thickness. Zircons were analyzed for U, Th, and Pb isotopes by LA-ICP-MS techniques at the Museum für Mineralogie und Geologie (GeoPlasma Lab, Senckenberg Naturhistorische Sammlungen Dresden), using a Thermo-Scientific Element 2 XR sector field ICP-MS coupled to a New Wave UP-193 Excimer Laser System. A teardrop-shaped, low volume laser cell constructed by Ben Jähne (Dresden) and Axel Gerdes (Frankfurt/M.) was used to enable sequential sampling of heterogeneous grains (e.g., growth zones) during time-resolved data acquisition. Each analysis consisted of approximately 15 s background acquisition followed by 30 s data acquisition, using a laser spot-size of 25 and 35 μm , respectively. A common-Pb correction based on the interference- and background-corrected ^{204}Pb signal and a model Pb composition (Stacey and Kramers, 1975) was carried out if necessary. The necessity of the correction is judged on whether the corrected $^{207}\text{Pb}/^{206}\text{Pb}$ lies outside of the internal errors of the measured ratios. Discordant analyses were generally interpreted with care. Raw data were corrected for background signal, common Pb, laser-induced elemental fractionation, instrumental mass discrimination, and time-dependant elemental fractionation of Pb/Th and Pb/U using an Excel® spreadsheet programme developed by Axel Gerdes (Institute of Geosciences, Johann Wolfgang Goethe-University Frankfurt, Frankfurt am Main, Germany). Reported uncertainties were propagated by quadratic addition of the external reproducibility obtained from the standard zircon GJ-1 (~0.6% and 0.5–1% for the $^{207}\text{Pb}/^{206}\text{Pb}$ and $^{206}\text{Pb}/^{238}\text{U}$, respectively) during individual analytical sessions and the within-run precision of each analysis. Concordia diagrams (2 sigma error ellipses) and concordia ages (95% confidence level) were produced using Isoplot/Ex 2.49 (Ludwig, 2001) and frequency and relative probability plots using AgeDisplay (Sircombe, 2004). The $^{207}\text{Pb}/^{206}\text{Pb}$ age was taken for interpretation for all zircons >1.0 Ga, and the $^{206}\text{Pb}/^{238}\text{U}$ ages for younger grains. Further details of the instruments settings are available from Table 1. For further details on analytical protocol and data processing see Gerdes and Zeh (2006).

The uncertainty in the degree of concordance of Precambrian-Palaeozoic grains dated by the LA-ICP-MS method is relatively large and results obtained from just a single analysis have to be interpreted with care. A typical uncertainty of 2–3% (2 sigma) in $^{207}\text{Pb}/^{206}\text{Pb}$ for a Late Neoproterozoic grain (e.g., 560 Ma) relates to an absolute error on the $^{207}\text{Pb}/^{206}\text{Pb}$ age of 45–65 Myr. Such a result gives space for interpretation of concordance or slight discordance. The latter one could be caused by episodic lead loss, fractionation, or infiltration Pb isotopes by a fluid or on micro-cracks. Thus, zircons showing a degree of concordance in the range of 90–110% in this paper are classified as concordant because of the overlap of the error ellipse with the concordia (Linnemann et al., 2011).

Th/U ratios are obtained from the LA-ICP-MS measurements of investigated zircon grains. U and Pb content and Th/U ratio were calculated relative to the GJ-1 zircon standard and are accurate to approximately 10%.

Appendix 2.

B.1. Geochemical analysis

Study of the carbon and oxygen stable isotope data from drilled limestone micro-samples (e.g., Kaufman and Knoll, 1995) was conducted at the University of Maryland Paleoclimate CoLaboratory using a refined method for the analysis and correction of carbon ($\delta^{13}\text{C}$) and oxygen ($\delta^{18}\text{O}$) isotopic composition of 100 μg carbonate

samples by continuous flow mass spectrometry (Spotl, 2011). Up to 180 samples loaded into 3.7 mL Labco Exetainer vials and sealed with Labco septa were flushed with 99.999% Helium and manually acidified at 60 °C. The carbon dioxide analyte gas was isolated via gas chromatography, and water was removed using a Nafion trap prior to admission into an Elementar Isoprime stable isotope mass spectrometer fitted with a continuous flow interface. Data were corrected via automated Matlab scripting on the Vienna Pee Dee Belemnite and LSVEC Lithium Carbonate (VPDB-LSVEC) scale (Coplen et al., 2006) using periodic in-run measurement of international reference carbonate materials and/or in-house standard carbonates, from which empirical corrections for signal amplitude, sequential drift, and one or two-point mean corrections were applied. Precision for both isotopes is routinely better than 0.1‰. Including acidification, flush fill, reaction and analysis, true throughput exclusive of correcting standards is 2–3 samples/hour, or up to 144 samples over a 40-h analytical session.

Sulphur abundance and isotope compositions of pyrite in acidified bulk samples and of a jarosite crust were determined by on-line combustion with a Eurovector elemental analyzer coupled to an Elementar Isoprime mass spectrometer. Prepared samples were accurately weighed and folded into small tin cups that were sequentially dropped with a pulsed O₂ purge of 12 ml into a catalytic combustion furnace operating at 1050 °C. The frosted quartz reaction tube was packed with high purity reduced copper wire for quantitative oxidation and O₂ resorption. Water was removed from the combustion products with a 10-cm magnesium perchlorate column, and the SO₂ was separated from other gases with a 0.8-m PTFE GC column packed with Porapak 50–80 mesh heated to 90 °C. The effluent from the elemental analysis (EA) was introduced in a flow of He (80–120 mL/min) to the IRMS through a SGE splitter valve that controls the variable open split. Timed pulses of SO₂ reference gas (Air Products 99.9% purity, ~3 nA) were introduced at the beginning of the run using an injector connected to the IRMS with a fixed open ratio split. The isotope ratios of reference and sample peaks were determined by monitoring ion beam intensities relative to background values. The cycle time for these analyses was 210 s with reference gas injection as a 30-s pulse beginning at 20 s. Sample SO₂ pulses begin at 110 s and return to baseline values between 150 and 180 s, depending on sample size and column conditions. Sulphur isotope ratios were determined by comparing integrated peak areas of *m/z* 66 and 64 for the reference and sample SO₂ pulses, relative to the baseline that is approximately $1 \times 10^{-11}\text{A}$. The background height was established from the left limit of the sample SO₂ peak. Isotopic results are expressed in the δ notation as per mil (‰) deviations from the Vienna Canyon Diablo Troilite (V-CDT) standard. Two NBS 127 barite standards and two IAEA NZ1 silver sulfide standards were measured between each set of 10 samples and uncertainties for each analytical session based on these standard analyses were determined to be better than 0.3‰.

For analysis of strontium isotopic composition, five limestone samples with visible aragonite pseudomorphs were chosen. Micro-drilled powders (ca. 5 mg) were leached three times in 0.2 M ammonium acetate (pH ~8.2) to remove exchangeable Sr from non-carbonate minerals, then rinsed three times in Milli-Q water. The leached powder was centrifuged, decanted, and acidified with doubly distilled 0.5 M acetic acid overnight to remove strontium from the carbonate crystal structure. The supernatant was centrifuged to remove insoluble residues and then decanted, dried, and subsequently dissolved with 200 μL of 3 M HNO₃. Strontium separation by cation-exchange was carried out using a small polyethylene column containing ~1 cm of Eichrom® Sr specific resin. The column was rinsed with 400 μL of 3 M HNO₃ before the dissolved sample was loaded onto the column. After loading, the sample was sequentially eluted with 200 μL of 3 M HNO₃, 600 μL of 7 M HNO₃ and 100 μL of 3 M HNO₃ to remove the Ca, Rb and REE fractions; the

Sr fraction adsorbs strongly to the resin in an acidic environment. The Sr fraction was removed by elution with ~800 μL of 0.05 M HNO₃ and the resultant eluate collected and dried. Approximately 200–300 mg of the dried sample was transferred onto a degassed and pre-baked (~4.2 Å under high vacuum) high purity Re filament with 0.7 μL of Ta₂O₅ activator. The prepared filaments were measured using the VG Sector 54 thermal ionization mass spectrometer at the University of Maryland Isotope Geochemistry Laboratory. Filaments were transferred to a sample carousel, heated under vacuum (~10⁻⁷ to 10⁻⁸ atm) to a temperature between 1450 and 1650 °C, and analyzed when a stable signal (>1.0 V) was detected on the ion beam of mass 88. Approximately 100 ⁸⁷Sr/⁸⁶Sr ratios were collected for each sample. Final data have been corrected for fractionation using the standard value ⁸⁶Sr/⁸⁸Sr = 0.1194. The fraction of ⁸⁷Sr resulting from *in situ* decay from ⁸⁷Rb was removed by measurement of rubidium abundance at mass 85. Repeated analysis of the NBS SRM987 standard yields an average value of ⁸⁷Sr/⁸⁶Sr = 0.71024448 ± 0.0000111(2σ) during the analytical window.

References

- Bladl, K.W., 1982. The formation of goethite, jarosite, and alunite during the weathering of sulfide-bearing felsic rocks. *Economic Geology* 77, 176–184.
- Canfield, D.E., Poulton, S.W., Narbonne, G.M., 2007. Late-Neoproterozoic deep-ocean oxygenation and the rise of animal life. *Science* 315, 92–95.
- Coplen, T., Brand, W.A., Gehre, M., Crooning, M., Meijer, H.A.J., Toman, B., Verkouteren, R.M., 2006. New guidelines for d¹³C measurements. *Analytical Chemistry* 78, 2439–2441.
- Corsetti, F.A., Kaufman, A.J., 2003. Stratigraphic investigations of carbon isotope anomalies and Neoproterozoic ice ages in Death Valley, California. *Geological Society of America Bulletin* 115, 916–932.
- Crimes, T.P., Germs, G.J.B., 1982. Trace fossils from the Nama Group (Precambrian–Cambrian) of Southwest Africa (Namibia). *Journal of Paleontology* 56, 890–907.
- Derry, L.A., Kaufman, A.J., Jacobsen, S.B., 1992. Sedimentary cycling and environmental change in the late Proterozoic: evidence from stable and radiogenic isotopes. *Geochimica et Cosmochimica Acta* 56, 1317–1329.
- Elliott, D.A., Vickers-Rich, P., Trusler, P., Hall, M., 2011. New evidence on the taphonomic context of the Ediacaran *Pteridinium*. *Acta Palaeontologica Polonica* 56 (3), 641–650.
- Fike, D., Grotzinger, J., Pratt, L., Summons, R., 2006. Oxidation of the Ediacaran ocean. *Nature* 444, 744–747.
- Frei, R., Graucher, C., Poulsen, S.W., Canfield, D.E., 2009. Fluctuations in Precambrian atmospheric oxygenation recorded by chromium isotopes. *Nature* 461, 250–253.
- Frei, R., Gaucher, C., Dossing, L.N., Sial, A.N., 2011. Chromium isotopes in carbonates – a tracer for climate change and for reconstructing the redox state of ancient seawater. *Earth and Planetary Science Letters* 312, 114–125.
- Gehling, J.G., 1999. Microbial mats in terminal Neoproterozoic siliciclastics: Ediacaran death masks. *Palaios* 14, 40–57.
- Gerdes, A., Zeh, A., 2006. Combined U-Pb and Hf isotope LA-(MC-) ICP-MS analysis of detrital zircons: comparison with SHRIMP and new constraints for the provenance and age of an Armorican metasediment in Central Germany. *Earth and Planetary Science Letters* 249, 47–61.
- Germs, G.J.B., 1972. The Stratigraphy and Paleontology of the Lower Nama Group, South West Africa, vol. 12. *Bulletin of the Precambrian Research Unit, University of Cape Town*.
- Germs, G.J.B., 1983. Implications of a sedimentary facies and depositional environmental analysis of the Nama Group in Southwest Africa/Namibia. In: Miller, R. McG. (Ed.), *Evolution of the Damara Orogen*, 11. Geological Society of South Africa, Special Publication, pp. 89–114.
- Germs, G.J.B., 1995. The Neoproterozoic of southwestern Africa, with emphasis on platform stratigraphy and paleontology. *Precambrian Research* 73, 137–151.
- Germs, G.J.B., Gresse, P.G., 1991. The foreland basin of the Damara and Gariep orogens in Namaqualand and southern Namibia: stratigraphic correlations and basin dynamics. *South African Journal of Geology* 94, 159–169.
- Germs, G.J.B., Knoll, A.H., Vidal, G., 1986. Latest Proterozoic microfossils from the Nama Group, Namibia (South West Africa). *Precambrian Research* 32, 45–62.
- Grant, S.W.F., 1990. Shell structure and distribution of *Cloudina*, a potential index fossil for the terminal Proterozoic. *American Journal of Science* 290-A, 261–294.
- Grahdankin, D., Seilacher, A., 2005. A re-examination of the Nama type Vendian organism *Rangea schneiderhoehni*. *Geological Magazine* 142, 571–582.
- Gresse, P.G., Germs, G.J.B., 1993. The Nama foreland basin: sedimentation, major unconformity bounded sequences and multisided active margin advance. *Precambrian Research* 63, 247–272.
- Grotzinger, J.P., Miller, R. McG., 2008. Nama Group. In: Miller, R. McG. (Ed.), *The Geology of Namibia*, vol. 2. Geological Survey of Namibia, pp. 13.229–13.272.
- Grotzinger, J.P., Bowring, S.A., Saylor, B.Z., Kaufman, A.J., 1995. New biostratigraphic and geochronologic constraints on early animal evolution. *Science* 270, 598–604.
- Grotzinger, J.P., Watters, W.A., Knoll, A.H., 2000. Calcified metazoans in thrombolite-stromatolite reefs of the terminal Proterozoic Nama Group, Namibia. *Paleobiology* 26, 334–359.
- Halvorsen, G.P., Dudas, F.O., Maloof, A.C., Bowring, S.A., 2007. Evolution of the ⁸⁷Sr/⁸⁶Sr composition of Neoproterozoic seawater. *Palaeogeography, Palaeoclimatology, Palaeoecology* 236, 103–129.
- Hayes, J.M., 1983. Geochemical evidence bearing on the origin of aerobiosis, a speculative interpretation. In: Schopf, J.W. (Ed.), *The Earth's Earliest Biosphere: Its Origin and Evolution*. Princeton University Press, NY.
- Hoffmann, K.H., 1989. New aspects of lithostratigraphic subdivision and correlation of late Proterozoic to early Cambrian rocks of the southern Damara Belt and their correlation with the central and northern Damara Belt and the Gariep Belt. *Communications of the Geological Survey of Namibia* 5, 59–67.
- Jacobsen, S.B., Kaufman, A.J., 1999. The Sr, C and O isotopic evolution of Neoproterozoic seawater. *Chemical Geology* 161, 37–57.
- Jambor, J.L., Blawes, D.W., 1998. Theory and applications of mineralogy in environmental studies of sulfide-bearing mine wastes. In: Cabri, L.J., Vaughan, D.J. (Eds.), *Modern Approaches to Ore and Environmental Mineralogy* 27. Mineralogical Association of Canada Short Course Series, Mineralogical Association of Canada, Ottawa, Canada, pp. 367–401.
- Johnson, H.D., Baldwin, C.T., 1986. Shallow siliciclastic seas. In: Reading, H.G. (Ed.), *Sedimentary Environments and Facies*. Blackwell, Boston, pp. 229–282.
- Kaufman, A.J., Hayes, J.M., Knoll, A.H., Germs, G.J.B., 1991. Isotopic compositions of carbonates and organic carbon from upper Proterozoic successions in Namibia: stratigraphic variation and the effects of diagenesis and metamorphism. *Precambrian Research* 49, 301–327.
- Kaufman, A.J., Jacobsen, S.B., Knoll, A.H., 1993. The Vendian record of Sr- and C isotopic variations in seawater: implications for tectonics and paleoclimate. *Earth and Planetary Science Letters* 120, 409–430.
- Kaufman, A.J., Knoll, A.H., 1995. Neoproterozoic variations in the carbon isotopic composition of seawater: stratigraphic and biogeochemical implications. *Precambrian Research* 73, 27–49.
- Kaufman, A.J., Knoll, A.H., Narbonne, G.M., 1997. Isotopes, ice ages, and terminal Proterozoic Earth history. *Proceedings of the National Academy of Sciences of the United States of America* 94, 6600–6605.
- Kimura, H., Watanabe, Y., 2001. Oceanic anoxia at the Precambrian-Cambrian boundary. *Geology* 29, 995–998.
- Knauth, L.P., Kennedy, M.J., 2009. The late Precambrian greening of the Earth. *Nature* 460, 728–732.
- Leonov, M.V., Fedonkin, M.A., Vickers-Rich, P., Ivantsov, A.Yu., Trusler, P., Hoffmann, K.H., 2010. Discovery of the first macroscopic carbonaceous algal assemblage in the Terminal Proterozoic of Namibia, southwest Africa. *Geological Survey of Namibia Publication* 14, 1–7.
- Ling, H.F., Chen, X., Li, D., Wang, D., Shields-Zhou, G.A., Zhu, M., 2013. Cerium anomaly variations in Ediacaran-earliest Cambrian carbonates from the Yangtze Gorges area, South China: Implications for oxygenation of coeval shallow seawater. *Precambrian Research* 225, 110–127.
- Linnemann, U., Ouzeqane, K., Drareni, A., Hofmann, M., Becker, S., Gärtner, A., Sagawe, A., 2011. Sands of West Gondwana: An archive of secular magmatism and plate interactions—A case study from the Cambro-Ordovician section of the Tassili Ouan Ahaggar (Algerian Sahara) using U-Pb LA-ICP-MS detrital zircon ages. *Lithos* 123, 188–203.
- Lottermoser, B.G., 2010. *Mine Wastes: Characterization, Treatment and Environmental Impacts*, 3rd ed. Springer-Verlag, Berlin, Germany.
- Ludwig, K.R., 2001. *Users Manual for Isoplots/Ex rev. 2.49*. Berkeley Geochronology Center Special Publication No. 1a, 1–56.
- Maloof, A., Rose, C., Beach, R., Samuels, B., Calmet, C., Erwin, D., Poirier, G., Yao, N., Simons, F., 2010. Possible animal-body fossils in pre-Marinoan limestones from South Australia. *Nature Geoscience* 3 (9), 653–659.
- McFadden, K.A., Jing Huang, Xuelei Chu, Ganqing Jiang, Kaufman, A.J., Chuanming Zhou, Xunhai Yuan, Shuhai Xiao, 2008. Redox instability and biological evolution in the Ediacaran Doushantuo Formation. *Proceedings of the National Academy of Sciences of the United States of America* 105, 3197–3202.
- Murray, H.H., 1988. Kaolin minerals: their genesis and occurrences. In: Bailey, S.W. (Ed.), *Hydrous Phyllosilicates (Exclusive of Micas)* 19. *Reviews in Mineralogy, Mineralogical Society of America*. Washington, DC, USA, pp. 67–89.
- Narbonne, G.M., Xiao, S., Shields, G., 2012. The Ediacaran Period, chapter 18. In: Gradstein, F., Ogg, J., Ogg, G. (Eds.), *Geologic Timescale 2012*. Elsevier, pp. 427–449.
- Narbonne, G.M., Saylor, B.Z., Grotzinger, J.P., 1997. The youngest Ediacaran fossils from southern Africa. *Journal of Paleontology* 71, 953–967.
- Pflug, H.D., 1966. Neue Fossilreste aus den Nama-Schichten in Sudwest-Afrika. *Palaeontologische Zeitschrift* 40, 14–25.
- Pflug, H.D., 1970a. Zur fauna der Nama-Schichten in Sudwest-Afrika. I. *Pteridinium*, *bau und systematische zugehörigkeit*. *Palaeontographica Abteilung A* 134, 226–262.
- Pflug, H.D., 1970b. Zur fauna der Nama-Schichten in Sudwest-Afrika. II. *Rangiae*, *bau und systematische Zugehörigkeit*. *Palaeontographica Abteilung A* 135, 198–231.
- Pflug, H.D., 1972. Zur fauna der Nama-Schichten in Sudwest-Afrika. III. *Ernitettomorphha*, *bau und systematic*. *Palaeontographica Abteilung A* 139, 134–170.
- Ries, J.B., Fink, D.A., Pratt, L.M., Lyons, T.W., Grotzinger, J.P., 2009. Superheavy pyrite ($\delta^{34}\text{S} > \delta^{34}\text{S}_{\text{cas}}$) in the terminal Proterozoic Nama Group, southern Namibia: a

- consequence of low seawater sulphate at the dawn of animal life. *Geology* 37, 743–746.
- Saylor, B.Z., 1993. Progress report on the sedimentology and stratigraphy of the Kuibis and Schwarrand Subgroups, Witputs area, southwestern Namibia. Geological Survey of Namibia, Communications 8, 127–135.
- Saylor, B.Z., Grotzinger, J.P., 1997. Reconstructions of important Proterozoic-Cambrian boundary exposures through the recognition of thrust deformation in the Nama Group of southern Namibia. Geological Survey of Namibia, Communications 11, 1–12.
- Saylor, B.Z., Grotzinger, J.P., Germs, G.J.B., 1995. Sequence stratigraphy and sedimentology of the Neoproterozoic Kuibis and Schwarrand subgroups (Nama Group), southwestern Namibia. *Precambrian Research* 73, 153–172.
- Saylor, B.Z., Kaufman, A.J., Grotzinger, J.P., Urban, F., 1998. A composite reference section for terminal Proterozoic strata of southern Namibia. *Journal of Sedimentary Research* 68 (6), 1223–1235.
- Saylor, B.Z., Poling, J.M., Huff, W.D., 2005. Stratigraphic and chemical correlation of volcanic ash beds in terminal Proterozoic Nama Group, Namibia. *Geological Magazine* 142 (5), 519–538.
- Schröder, S., Grotzinger, J.P., 2007. Evidence for anoxia at the Ediacaran–Cambrian boundary: the record of redox-sensitive trace elements and rare earth elements in Oman. *Journal of the Geological Society, London* 164, 175–187.
- Shen, B., Xiao, S., Kaufman, A.J., Bao, H., Zhou, C., Wang, H., 2008. Sulfur isotopes of the basal Ediacaran Zhamoketi cap carbon in Qurutagh Area, Chinese Tianshan: Implications for sulfur cycling in a post-Marinoan basin. *Earth and Planetary Science Letters* 265, 209–228.
- Sircombe, K.N., 2004. AgeDisplay: An EXCEL workbook to evaluate and display univariate geochronological data using binned frequency histograms and probability density distributions. *Computers & Geosciences* 30, 21–31.
- Spotl, C., 2011. Long-term performance of the Gasbench isotope ratio mass spectrometry system for the stable isotope analysis of carbonate microsamples. *Rapid Communications in Mass Spectrometry* 25, 1683–1685, <http://dx.doi.org/10.1002/rcm.5037>.
- Squyres, S.W., Grotzinger, J.P., Arvidson, R.E., Bell III, J.F., Calvin, W., Christensen, P.R., Clark, B.C., Crisp, J.A., Farrand, W.H., Herkenhoff, K.E., Johnson, J.R., Klingelhofer, G., Knoll, A.H., McLennan, S.M., McSween Jr., H.Y., Morris, R.V., Rice Jr., J.W., Rieder, R., Soderblom, L.A., 2004. In situ evidence for an ancient aqueous environment at Meridiani Planum. *Mars Science* 306 (5702), 1709–1714.
- Stacey, J.S., Kramers, J.D., 1975. Approximation of terrestrial lead isotope evolution by a two-stage model. *Earth and Planetary Science Letters* 26, 207–221.
- Vickers-Rich, P., Ivantsov, A.Y., Trusler, P., Narbonne, G.M., Hall, M., Wilson, S.I., Greentree, C., Fedonkin, M.A., Elliott, D.A., Hoffmann, K.H., Schneider, G.I.C., 2013. Reconstructing Rangea: new discoveries from the Ediacaran of southern Namibia. *Journal of Paleontology* 87 (1), 1–15.
- Walker, R.G., Plint, A.G., 1992. Wave- and storm-dominated shallow marine systems. In: Walker, R.G., James, N.P. (Eds.), *Facies Models: Response to Sea Level Change*. Geological Association of Canada, St John's, pp. 219–238.
- Zecchin, M., 2007. The architectural variability of small-scale cycles in shelf and ramp clastic systems: The controlling factors. *Earth-Science Reviews* 84, 21–25.